NASA Contractor Report 172498

STRESSES IN PIN-LOADED ORTHOTROPIC PLATES USING PHOTOELASTICITY

M. W. Hyer and D. Liu

VIRGINIA POLYTECHNIC INSTITUTE AND STATE UNIVERSITY
Blacksburg, VA 24061

Grant NSG-1621
October 1984

National Aeronautics and
Space Administration

Langley Research Center
Hampton, Virginia 23665

STRESSES IN PIN-LOADED ORTHOTROPIC PLATES USING PHOTOELASTICITY

M. W. Hyer[1]

Department of Engineering Science and Mechanics
Virginia Polytechnic Institute and State University
Blacksburg, Virginia 24061

and

D. Liu[2]

Department of Engineering Science
University of Florida
Gainesville, FL 32611

(1) Professor

(2) Research Associate, formerly graduate student at VPI & SU

Abstract

The stresses in transparent glass-epoxy plates loaded by a steel pin through a hole were determined experimentally using photoelasticity. The paper presents the stresses around the hole edge, across the net section, along the shear-out line, and on the centerline below the hole for quasi-isotropic, unidirectional, and angle-ply plates. Stresses in an isotropic comparison specimen are also presented. Stress concentration factors for several locations around the plates are tabulated. The paper discusses the experimental apparatus and the experimental technique. The isochromatic and isoclinic fringe patterns for the four plates are shown. An appendix presents the necessary photoelastic theory.

INTRODUCTION

There have been many numerical studies aimed at determining the stress distribution around a pin-loaded hole in an orthotropic plate [1-12]. This paper presents the results of an experimental study, the stress distribution being determined by means of photoelasticity. The photoelastic technique is based on the phenomenon of birefringence and requires the plate to be transparent. Therefore this study was limited to the determination of the stresses in glass-epoxy plates. Specifically, the stresses in three laminated glass-epoxy plates were determined. These plates were: a quasi-isotropic plate with a lay-up of $(0_4/45_4/-45_4/90_4)_S$; a unidirectional $0°_{32}$ plate; and angle-ply $(+45_4/-45_4)_{2S}$ plate. Since it is a subject in its own right, photoelasticity as it is applied to fiber-reinforced materials is addressed in an appendix. The paper itself describes the experimental apparatus used to load the glass-epoxy plates by means of a pin through a hole. Some of the details of the experimental procedure are presented. Typical isochromatic and isoclinic fringes are illustrated. The radial and hoop stresses around the hole, net-section tensile stresses, shear-out stresses below the hole, and stresses along the centerline below the hole are presented. A compilation of stress concentration factors is also presented. For purposes of comparison, similar results for a homogeneous isotropic plate, tested at the same time, are presented.

EXPERIMENTAL SET-UP

Figure 1 shows a schematic of the arrangement used to load the plates. The width, W, of each plate was 203 mm and they were 292 mm long. The glass-epoxy plates were 2.29 mm thick while the isotropic plate was 3.00 mm thick. The hole diameter, D, in each plate was 50.8 mm and the distance from the center of the hole to the free end, e, was 101 mm. With these dimensions the

plate-width to hole-diameter ratio, W/D, was 4 while the end-distance to hole-diameter ratio, e/D, was 2. These two dimensionless parameters are frequently used to describe single-hole joint geometry. The volume fraction of glass in the plates was between 50 and 60% and the test specimens were cut from panels fabricated by IITRI [13] using a diamond saw. The large hole was drilled with an ultrasonic core drill. Care had to be taken to insure the cutting and drilling operation did not generate excess heat. Heat would generate residual stresses at the hole edge, and the bottom and sides of the plate. This could significantly affect the experimental determination of stresses. Thus water-based coolants were used during the cutting and drilling operations. The cutting and drilling times were short so that adsorption of the coolant by the specimens was not a problem. Table 1 presents the mechanical properties of the three glass-epoxy plates and the one isotropic comparison plate. The isotropic plate was polycarbonate, specifically PSM-1*. For a photoelastic stress analysis these mechanical properties are not necessary. They are included here for completeness. The material properties of each plate that are necessary are the stress-optic coefficients. These are discussed and given in the Appendix.

To one end of each plate were attached two aluminum load-introduction plates. These plates were 3.18 mm thick, 240 mm long, and 203 mm wide. They were attached to the glass-epoxy plates with small no. 10 bolts. The load, P, was introduced into the upper end of the aluminum plates by a smooth steel

* available from Measurements Group, Inc., Photolastic Division, P.O. Box 27777, Raleigh, NC 27611.

pin. The aluminum plates served to distribute the concentrated load P evenly into the glass-epoxy. In this manner the limited supply of glass-epoxy was not being used to simply smooth the load introduction

Table 1

Mechanical Properties of Plates

specimen property	Isotropic[1]	quasi-isotropic[2]	undirectional[2]	angle-ply[2]
E_x, GPa	1.38	19.7	37.2	12.4
E_y, GPa	1.38	19.7	12.3	12.4
G_{xy}, GPa	0.490	7.38	3.93	10.9
ν_{xy}	0.4	0.328	0.300	0.577

(1) from material supplier, see footnote on previous page.

(2) from ref. 13.

The pin was steel, of a snug fit, and the load was introduced to it by two steel crossbars. Since primary interest was in the stresses to the side and below the hole, no attempts were made to load the pin in such a manner that the region above the pin was observable. The two steel cross-bars were in turn loaded by the two steel U-shaped yokes which transmitted the load. Smooth steel pins were used to join the crossbar and yoke and to transmit the load at the lower end of the assembly. A loading frame which utilized dead weights was used to load the specimen.

The specific load levels used in the testing were a compromise between wanting to use enough load to generate a sufficient number of fringes but yet not cause local damage to the specimen. Local damage such as matrix cracking in a ply would scatter the light, change the optical calibration, or even render the glass-epoxy opaque. Therefore, damage was to be avoided. All data

reported here for the three glass-epoxy specimens were recorded at a load P of 5.92 kN. The load used for the isotropic specimen was 1.56 kN.

FRINGE DETERMINATION

The key to an accurate photoelastic stress analysis is being able to record the isochromatic and isoclinic fringes. As explained in the Appendix, fringe definition with the glass-epoxy material is not as sharp as it is with standard homogeneous isotropic photoelastic materials. The scattering of light passing through the material and the low birefringence sensitivity of the composite material are the primary causes of the poor fringe definition. In addition, in some circumstances residual birefringence contributes to the isochromatic and isoclinic fringe pattern and so the isoclinic fringes have to be determined in the presence of the full isochromatic fringe pattern. As a result, the fringe recording and interpretation portion of these photoelastic experiments was a significant portion of the total effort. To aid in the determination of the fringes, high contrast film was used. Specifically Kodak Ortho Contrast 101 x 127 mm negative film was used for recording the isoclinics. The isochromatics were recorded on a standard film. One exposure of high contrast film was required for each isocline fringe measured. For those situations when residual birefringence effects were important, the isochromatic fringe pattern and isoclinic fringe pattern were recorded simultaneously in white light. Since in white light the isochromatics are colored and the isoclinics are black, overexposure of high contrast film washed out the isochromatics and the result was a relatively clear picture of the isoclinic.

TYPICAL FRINGE PATTERNS

Figures 2-5 show the isochromatic fringe patterns for the isotropic, quasi-isotropic, unidirectional, and angle-ply specimens respectively. The results from the isotropic comparison specimen are shown first for several reasons. First, this specimen, with its relatively high fringe density, was used to check alignment of the loading apparatus. Symmetry of the loading, or lack of it, about the vertical centerline could be checked by visually examining the symmetry of the isochromatic fringe pattern. There were no adjustment mechanisms built into the loading apparatus. However, with proper machining none would be necessary. As can be seen from the symmetry of the fringe pattern in fig. 2, alignment was not a problem. The second reason for showing the isotropic case first is to show that the density of fringes encountered using standard isotropic material is high when compared to the density of fringes using glass-epoxy. Also, the fringes are sharp and clear. The lower fringe density in the isochromatic fringe patterns of figs. 3-5 for the glass-epoxy, despite the higher loads, attests to the lower birefringence sensitivity of that material. The lack of sharp fringes in the glass-epoxy is evident. Finally, the isotropic specimen was actually tested first, acting as a 'dry run' for the entire test procedure, including fringe recording and stress determination. The stresses from this more traditional case served as a basis for comparison with the cases.

There are several interesting features to the isochromatic fringes of the glass-epoxy specimens. First, for the quasi-isotropic case there was a slight asymmetry to the fringes. This was more pronounced near the hole. In light of the symmetry of the fringes exhibited by the isotropic material, the lack of symmetry was puzzling and was attributed to spatial variations in material properties, particularly the optical properties, of the glass-epoxy. Because

of this lack of symmetry, the photoelastic analysis was conducted by averaging fringe data on both sides of the centerline. The averaged data were then used in a symmetric analysis of the right sides of the plates. As far as overall shape is concerned, the fringe patterns for the quasi-isotropic specimen were quite similar to the fringe patterns for the isotropic specimen. In fact, tests on quasi-isotropic disks indicated the material was optically isotropic.

The isochromatic fringes associated with the unidirectional plate were significantly elongated in the direction of the fibers. There was a slight amount of asymmetry and again, this was attributed to spatial variations in the material itself. There was about 0.1 residual fringe in the unidirectional material. As can be seen from the figure of the unidirectional material, the fibers tended to smear the fringes.

The fringe pattern in the angle-ply specimen behaved as expected, i.e. showing some sort of distinct behavior in the direction of the fibers. From figs. 2-5 it is evident that fringe determination was more of an issue in the glass-epoxy materials than in standard photoelastic materials.

A typical isocline is shown in fig. 6. This is the 30° isocline in the quasi-isotropic laminate and the pattern was recorded with the high contrast film. Figures 7-10 show the isoclines in 5° increments for all four specimens. These figures were constructed by tracing the results of isoclinic photographs similar to fig. 6 on a common piece of paper. From figs. 6 it is obvious judgement was required in determining the exact center of the fringe. There was a lack of perfect symmetry in the isoclinic pattern for all cases and the isotropic and quasi-isotropic isocline characteristics were quite similar. The isoclinics for the unidirectional case were clustered more directly beneath the hole while the isoclinics for the angle-ply were clustered in the ±45° directions. From the point of view of data reduction, the clustering of

isoclines was not desirable. With clustering, a small error in spatial location led to a large error in determining the isocline angle.

STRESS COMPUTATIONS

The stresses over the right hand portion below the net section were computed for each plate by the method described in the Appendix. In this paper the stresses at the hole edge and along several important loci emanating from the hole edge are reported. Stresses at other locations can be found in ref. 14. Specifically, referring to fig. 11, stresses along hole-edge arc AE, and lines AB, EC, and ED are reported. Line AB is the centerline and experiences bearing stresses. Line EC is referred to as the shear-out line while line ED is the net-section line. The loci are important because the net section near the hole is the region of tensile failure, the centerline under the hole is the site of bearing failures, and the shear-out line is the location of shear-out failures. Only the dominant stress along each locus is shown, compressive stresses along the centerline, tensile stresses along the net-section locus, and shear stresses along the shear-out locus. Before the stresses are presented, an important check which was conducted on the experimentally determined results is discussed.

To assess the overall validity of the experimentally determined stresses, force equilibrium was checked at various locations on the specimen. Along the net section the integral of the tensile stresses should be directly related to the total applied load. Specifically

$$2t\int_{ED}\sigma_y dx = P, \qquad (1)$$

where t is the specimen thickness and P is the total applied load (see fig.

1). This assumes, correctly, that the pin contact angle is less than 180°. Similarly, along the shear-out locus below the hole,

$$2t \int_{EC} \tau_{xy} dy = P. \tag{2}$$

For any horizontal line below the hole

$$\int \sigma_y dx = 0. \tag{3}$$

Here the integral goes from the centerline to the right outside edge. This integral being zero reflects the fact that the hole reacts all the applied load and there is not net vertical load below the hole. The stresses around the hole edge could be checked for consistency in a similar manner. There the stresses were written in polar coordinates and equilibrium yields

$$2Dt \int_{AE} (\sigma_r \cos\theta + \tau_{r\theta} \sin\theta) d\theta = P. \tag{4}$$

Using the computed stresses, the above integrals were evaluated using Simpson's rule. The values of the integrals were divided by the actual load and the ratio was used as a measure of overall accuracy of the stress calculations.

Figure 12 shows the stresses at the hole edge for the isotropic comparison plate. The radial, σ_r, circumferential, σ_θ, and friction-induced shear, $\tau_{r\theta}$, stresses are shown as a function of circumferential location. For comparison, the $4/\pi \cos(\theta)$ radial stress distribution introduced by Bickley [15] and often used in numerical schemes is shown. The stresses are nondimensionalized by the bearing stress S, S being defined as

$$S = P/Dt \ . \qquad (5)$$

Figure 13 shows the stresses in the comparison isotropic plate along the three loci emanating from the hole edge. Figures 14-19 show similar information for the three glass-epoxy specimens. All data are plotted on a common scale for ease of comparison.

Referring to figs. 12-15, it is seen there was a similarity between the stresses in quasi-isotropic glass-epoxy and the stresses in the isotropic material. This was expected. Around the hole edge the radial and circumferential stresses in the glass-epoxy are quite close to their counterparts in the isotropic specimens. The shear stresses have a different sign, a difference that has not been explained. Also, in the glass-epoxy the bearing stress under the hole was higher than it was in the isotropic material. In either case the $4/\pi \cos(\theta)$ only roughly approximates the measured radial stress distribution. The cosinusoidal distribution is more skewed to the $\theta = 0$ position than is the measured distribution. The maximum radial stress did not occur at $\theta = 0$, as the $4/\pi \cos(\theta)$ distribution assumes, rather the peak radial stress is off the centerline. The reduced radial stress at $\theta = 0$ is due to friction effects and has been documented analytically by Hyer and Klang [12] and by de Jong [16]. Table 2 summarizes the stress concentration factors, based on bearing stress, for the isotropic, quasi-isotropic, and other specimens. The table also indicates the location of the maximum hoop and radial stresses. Table 3 summarizes the results of the equilibrium checks for the specimens. For the isotropic specimens the results were about 10% too low for the loci with net loads and very good, 0.1%, for loci with no net load. The quasi-isotropic specimen integrals were as good if not slightly better for the

Table 2

Stress Concentration Factors

	isotropic	quasi-isotropic	unidirectional	angle-ply
σ_θ/S @ E	1.20	1.11	1.95	1.24
σ_r/S @ A	0.87	1.07	0.94	0.822
max τ_{xy}/S	0.50	0.55	0.44	0.69
location along EC(1) in mm	19.0	19.0	19.0	12.7
max σ_θ/S	1.20	1.11	1.95	1.29
location along AE(2)	90°	90°	90°	70°
max σ_r/S	0.93	1.09	1.01	1.06
location along AE(2)	37.5°	15°	45°	45°

(1) along shear-out locus, measured from net-section.
(2) θ = 0 on centerline.

loaded loci and also good, < 5%, for the unloaded loci.

The stress calculations for the unidirectional specimen are shown in figs. 16 and 17. At the hole edge, fig. 16, there were interesting differences between the quasi-isotropic case and the unidirectional case. For the unidirectional specimen the friction-induced shear stress actually reversed sign several times around the circumference. However, the most interesting difference was in the hoop stress. The hoop stress remained low from $\theta = 0$ to $\theta = 50°$ and then increased rapidly to a maximum at the net section. In contrast, the hoop stress for the quasi-isotropic specimen increased steadily from $\theta = 0$ to $\theta = 90°$. This behavior in orthotropic materials has been shown qualitatively by analysis for graphite-epoxy [7,12,16]. However, quantitative comparisons between those works and the present one are not meaningful. The ratio of fiber-direction to matrix-direction stiffness is 20:1 for graphite-epoxy whereas it was 3:1 for the glass-epoxy used here. Quantitatively, the 20:1 ratio produces significantly different effects than a 3:1 ratio, all other parameters being equal.

Table 3

Equilibrium Integrals

$\frac{\text{Value of integral}}{P_{\text{actual}}} \times 100\%$

specimen location	isotropic	quasi-isotropic	unidirectional	angle-ply
net section, eq. 1	93%	104%	89%	112%
shear-out, eq. 2	90%	96%	95%	109%
horizontal line below hole, eq. 3 (line C-C, Appendix Fig. A1)	0.1%	1.3%	1.2%	2.6%
contact region on hole edge, eq. 4	90%	91%	91%	106%

At the net section, fig. 17, the stresses at the hole edge in the unidirectional specimen were much higher than for the quasi-isotropic specimen. The shear-out stresses were similar to the quasi-isotropic case, as were the compressive stresses on the centerline below the hole. It was surprising that the bearing stress directly below the hole was not higher for the unidirectional case than for the quasi-isotropic case. It was felt the greater stiffness of the material in the loading direction for the unidirectional case would load the bottom of the hole more than for the quasi-isotropic case. This would be true if the shear stiffness of the unidirectional specimen was the same as the shear stiffness of the quasi-isotropic specimen. The unidirectional specimen shear stiffness was actually much less and so the 'plug' of material below the hole simply moved down as a rigid piece due to weak shear stiffness along the shear-out line. Such a unidirectional specimen would fail by the shearing out of the plug of material below the pin.

An interesting feature occurred in the unidirectional specimen at the net section. Despite the need to transmit a tensile force through the net section, at the outside edge the σ_y stresses were actually compressive. The compressive stresses are a characteristic of the response of orthotropic materials loaded in the stiff direction. The compression is necessary because the material overreacts in tension to the presence of the hole. The lack of stiffness perpendicular to the fibers does not permit the material to respond to the presence of the hole with as much spatial uniformity as, say, an isotropic material.

As can be seen from Table 2, the net-section stress concentration factor for the unidirectional specimen was the highest among the specimens and the maximum hoop stress occurred at the net section. The maximum radial stress occurred at $\theta = 45^{o}$. The numerical evaluation of the equilibrium integrals,

shown in Table 3, indicates the overall accuracy was similar to the accuracies of the two previous cases.

Finally, figs. 18 and 19 show results from the angle-ply case. The hoop stress around the hole, fig. 18, started negative at $\theta = 0$, increased to a maximum around 70°, then dropped off slightly. This behavior was not exhibited by the other specimens but the slightly negative hoop stress at $\theta = 0$ has been observed in numerical studies [12,16] and is due to friction. Overall the radial stress was similar to the other cases and was different than the cosinusoidal idealization.

CONCLUDING COMMENTS

Presented has been experimental data heretofore lacking. The data were obtained from plates which were realistic representations of actual structural elements. The volume fraction of fibers was similar to the value encountered in typical applications of glass-epoxy. It would have been ideal if the degree of orthotropy approached that of graphite-epoxy. It did not and so the data must be viewed in that context. If that is done the data can be useful. Also, there is no question that the numerical results presented were affected by fringe interpretation errors, material calibration errors, and numerical errors in the data reduction scheme described in Appendix A. This must also be kept in mind when viewing the data. However, the equilibrium integral checks did show that, overall, the experimental results were consistent and the chance of a large error in the results is low.

ACKNOWLEDGEMENTS

The research effort which led to the results presented here was financially supported by the Structures Laboratory, USARTL (AVSCOM). The technical monitor was Donald J. Baker, NASA Langley Research Center.

References

1) J. P. Waszczak, T. A. Cruse, "Failure Mode and Strength Predictions of Anisotropic Bolt Bearing Specimens," J. Comp. Mat., Vol. 5, July 1971, pp. 421-425.

2) D. W. Oplinger, K. R. Gandhi, "Stresses in Mechanically Fastened Orthotropic Laminates," 2nd Conf. of Fib. Comp. in Flight Vehicle Design, May 1974, pp. 813-841.

3) D. W. Oplinger, K. R. Gandhi, "Analytical Studies of Structural Performance in Mechanically Fastened Fiber-Reinforced Plates," Army Symp. on Solid Mech., Sept. 1974, pp. 211-240.

4) T. de Jong, "Stresses Around Pin-Loaded Holes in Elastically Orthotropic or Isotropic Plates," J. Comp. Mat., Vol. 11, July 1977, pp. 313-331.

5) Agarwal, B. L., "Static Strength Prediction of Bolted Joint in Composite Material," AIAA Journal, vol. 18, Nov. 1980, pp. 1371-1375.

6) S. P. Garbo, J. M. Ogonowski, "Effect of Variances and Manufacturing Tolerances on the Design Strength and Life of Mechanically Fastened Composite Joints," AFWAL-TR-81-3041, Vols. 1-3, April 1981.

7) Crews, J. H., Jr., Hong, C. S., and Raju, I. S., "Stress Concentration Factors for Finite Orthotropic Laminates with a Pin-Loaded Hole," NASA TP-1862, May 1981.

8) Wong, C. M. S. and Matthews, F. L., "A Finite-Element Analysis of Single and Two-Hole Bolted Joints in Fibre Reinforced Plastic," J. Composite Materials, vol. 15, 1981, pp. 481-491.

9) R. E. Rowlands, M. U. Rahman, T. L. Wilkinson, Y. I. Chiang, "Single- and Multiple-Bolted Joints in Orthotropic Materials," Composites, Vol. 13, No. 3, July 1982, pp. 273-278.

10) F. L. Matthews, C. M. Wong, S. Chryssafitis, "Stress Distribution Around a Single Bolt in Fibre-Reinforced Plastic," Composites, Vol. 13, No. 3, July 1982, pp. 316-322.

11) F. K. Chang, R. A. Scott, G. S. Springer, "Strength of Mechanically Fastened Composite Joints," J. Comp. Mat., Vol. 16, Nov. 1982, pp. 470-494.

12) Hyer, M. W. and Klang, E. C., Stresses in Pin-loaded Orthotropic Plates, Virginia Polytechnic Institute and State University, Center for Composite Materials and Structures, Report No. CCMS-84-02, 1984.

13) Daniels, I. M., Niro, T., and Koller, G. M., "Development of Orthotropic Birefringent Materials for Photoelastic Stress Analysis," NASA CR-165709, May 1981.

14) Liu, D., Stress Analysis of Pin-Loaded Orthotropic Plates Using Orthotropic Photoelasticity, Ph.D. Thesis, Department of Engineering Science and Mechanics, Virginia Polytechnic Institute and State University, 1984.

15) Bickley, W. G., "The Distribution of Stress Round a Circular Hole in a Plate," Phil. Trans. Royal Society, A (London), vol. 227, July 1928, pp. 383-415.

16) T. de Jong, "The Influence of Friction on the Theoretical Strength of Pin-Loaded Holes in Orthotropic Plates," Rep. No. LR-350, Dept. of Aerospace Engr., Delft Univ. Tech., March 1982.

APPENDIX

Stress Determination in Fiber-Reinforced Composites Using Photoelasticity

INTRODUCTION

Because of its success in aiding in the study of stresses in structural and mechanical components made of isotropic material, transmission photoelasticity has been extended to study stresses in fiber-reinforced materials. The terms orthotropic photoelasticity and orthophotoelasticity have been applied to the subject. Because structural components fabricated from fiber-reinforced materials are generally made of laminates which are much thinner than they are long and wide, the two-dimensional plane-stress analysis associated with transmission photoelasticity in isotropic materials also applies in the case of orthotropic fiber-reinforced materials. Obviously there is a limited class of materials for which the phenomenon can be used, the main requirement being that both the fiber and the matrix be transparent. In addition, the index of refraction of the fiber must closely match the index of refraction of the matrix or else the light scatters when it is transmitted through the composite. The early work in orthotropic photoelasticity centered on the development of materials [A1] and the development of appropriate stress-optic laws [A1-A7]. At this point, acceptable stress-optic laws have been established and techniques for making the material have been refined [A8,A9].

The material generally consists of a glass fiber embedded in a resin matrix. Fiber volume fractions in excess of 50% fiber are possible and for the most part the material is fabricated much like other resin-matrix composites, requiring elevated temperature and a vacuum to cure. The final product is a

thin transparent laminate and the optical properties for light transmitted through the thickness are a through-the-thickness average of the properties of the glass and resin. For purposes of analysis the laminate is considered an equivalent homogeneous but orthotropic material. This is much like the situation when considering inplane mechanical properties of fiber-reinforced materials. In actual application orthotropic photoelasticity is not as accurate or as easy to use as its classical isotropic counterpart. There are several reasons for this [A10]. First, the fiber-reinforced material fabricated so far is much more insensitive to the photoelastic effect than typical isotropic photoelastic material, e.g. PSM-1.* The sensitivity of the fiber-reinforced material is 5-10 times less than the sensitivity of isotropic photoelastic material and thus there is a factor of 5-10 fewer fringes with which to work. Much more interpolation between fringes is necesary with the fiber-reinforced material, resulting in less experimental accuracy. The second reason for the less accurate nature of orthotropic photoelasticity is the tendency of the light to scatter as it is transmitted through the material. The scattered light leads to wide and sometimes poorly-defined fringes. A high degree of refractive index matching between the fiber material and the matrix material is necessary but perfect matching in the cured state is not possible. In addition, high stresses near the fiber-matrix interface, or even slightly different material properties there, cause local effects which lead to scattering of the light as it passes near and through the fiber. The scattering is due to the fact that in reality, the material does not behave optically exactly like an equivalent homogeneous material. Thirdly, and to a

* available from Measurements Group, Inc., Photolastic Division, P.O. Box 27777, Raleigh, NC 27611.

lesser degree, the lack of a constant volume fraction from one location to the next in the material can lead to inaccuracies. The optical sensitivity of the material depends on the volume fractions of fiber, resin, and voids. These can vary slightly from point to point in the materials. If a single set of stress-optic constants is applied to a given batch of material, as is usually done, inaccuracies result. In contrast, available isotropic photoelastic materials are extremely uniform in their properties. Finally, with fiber-reinforced materials there is the issue of residual birefringence. The elevated temperatures associated with curing the material, even if the temperatures are due to the exothermic reactions of a room-temperature cure epoxy, lead to residual stresses in the final product. These stresses lead to fringes even though the material is free of mechanically induced stresses. When mechanical loads are applied more fringes result. It is only the difference in the two fringe states that is of interest for determining mechanically induced stresses.

The next section presents the stress-optic laws for fiber-reinforced composite materials and discusses the method for determining numerical values of stress from the optical data.

STRESS-OPTIC LAW

The speed of propagation of light in a transparent material is related to the material's dielectric properties. The dielectric properties are tensor quantities, with principal values and principal directions. When a transparent material is subjected to a mechanical load, the dielectric properties change from their no-load values. Generally the applied load changes the dielectric tensor so that its principal values are unequal. Light polarized in one of the tensor's principal directions propagates through the material at a

different speed than light polarized in one of the other principal directions. By passing the two polarized light beams with different velocities through the proper optical elements, the beams can be made to interfere. When viewing a stressed photoelastic model the interference results in fringes appearing on the model. It is the purpose of the polariscope to provide the two incident polarized light beams to the model, and to provide the optical elements to effect interference of the two beams emerging from the model at different speeds. There are two sets of fringes associated with the stressed model, the isochromatic fringe, here denoted by N, and the isoclinic fringe, denoted by θ. The notation θ is used because the isoclinic fringe gives information about the principal directions of the dielectric tensor. Oftentimes the isocline is directly related to the principal stress direction in the stressed material.

Consider a stressed fiber-reinforced material with orthotropic mechanical and optical properties and with the material's principal elastic axes aligned with an x-y coordinate system. The relations between the isochromatic and isoclinic fringe numbers and the stresses at a point in this coordinate system are:

$$\frac{\sigma_x}{f_x} - \frac{\sigma_y}{f_y} = N_T\cos(2\theta_T) - N_R\cos(2\theta_R) \qquad \text{(A1a)}$$

$$\frac{\tau_{xy}}{f_{xy}} = \frac{N_T}{2}\sin(2\theta_T) - \frac{N_R}{2}\sin(2\theta_R). \qquad \text{(A1b)}$$

Here N_T is the isochromatic fringe number at the point, θ_T the isocline, N_R is the residual isochromatic fringe number, and θ_R is the residual isocline. The

term residual, subscript R, applies to the state when no mechanical loads are applied. The subscript T refers to the state of total birefringence, residual plus mechanically induced. The values of N_R and θ_R are determined prior to applying the load. The quantities f_x, f_y, and f_{xy} are the material's stress-optic coefficients and they also are determined by prior calibration. The angles θ_T and θ_R are measured relative to the +x axis. Equations A1 are referred to as stress-optic equations. The stress-optic relations can be referred to another coordinate system, for example an r-θ coordinate system rotated an angle θ from the x-y system. The angle θ is measured counterclockwise from the +x axis to the +r axis. Using standard transformations, eqs. A1a and b transform as

$$\frac{\sigma_r}{c_1} - \frac{\sigma_\theta}{c_2} + \frac{\tau_{r\theta}}{c_3} = N_T \cos(2\theta_T) - N_R\cos(2\theta_R) \tag{A2a}$$

$$\frac{\sigma_r - \sigma_\theta}{c_4} + \frac{\tau_{r\theta}}{c_5} = \frac{N_T}{2} \sin(2\theta_T) - \frac{N_R}{2} \sin(2\theta_R). \tag{A2b}$$

Here

$$\frac{1}{c_1} = \frac{\cos^2\theta}{f_x} - \frac{\sin^2\theta}{f_y} \tag{A3a}$$

$$\frac{1}{c_2} = \frac{\cos^2\theta}{f_y} - \frac{\sin^2\theta}{f_x} \tag{A3b}$$

$$\frac{1}{c_3} = 2\left(\frac{1}{f_x} + \frac{1}{f_y}\right)\sin\theta\cos\theta \tag{A3c}$$

$$\frac{1}{c_4} = -\frac{\sin\theta\cos\theta}{f_{xy}} \tag{A3d}$$

$$\frac{1}{c_5} = \frac{\cos^2\theta - \sin^2\theta}{f_{xy}}. \tag{A3e}$$

Both forms of the stress-optic equations, A1 and A2, were used here.

The key issue is that at each point in a loaded material there are three stresses to be determined, σ_x, σ_y, τ_{xy} or σ_r, σ_θ, $\tau_{r\theta}$. At each point there are only two quantities of experimental data, N_T and θ_T. (As stated previously, N_R, θ_R, f_x, f_y, f_{xy} are known a priori and are considered material properties). Thus there is one less item of experimental information at each point than there are unknown stresses. Traditionally experimentalists have relied on a third experimental measure at the point, such as measuring the thickness change with an interferometer, or they have used auxiliary conditions the stresses must satisfy. The latter is the approach used here. The determination of all three stress components is termed separation of stresses. The section below describes how it was done in this study.

STRESS-SEPARATION SCHEME

At each point in the pin-loaded plate, the stresses, in addition to satisfying the stress-optic equations A1 or A2, had to satisfy the plane stress equilibrium equations. The stress-optic equations are algebraic equations. The two equilibrium equations are first-order partial differential equations. Using a finite-difference representation of each equilibrium equation resulted in two other algebraic equations. The stresses had to satisfy these equations also. Using simple forward, backward, or central difference representations, the equilibrium equations involved stresses from neighboring points. With two stress-optic equations and two equilibrium equations in finite-difference form, there were four algebraic equations the three stress components at a point had to satisfy. If this pattern was repeated from point to point on a finite-difference mesh superposed on the plate, there resulted many more equations the stress components, at the mesh points, had to satisfy than there were unknown stress components. In addition, there were boundary conditions

the stresses had to satisfy. This resulted in an overdetermined set of linear algebraic equations. The solution to these equations satisfied all equations in a least-squares sense.

Figure A1 illustrates a plate with a rectangular finite-difference mesh superposed on the right half. The meshes are divided into zones and there are different densities to the meshes. Figure A2 shows a polar mesh surrounding one-half the hole. The zones are numbered 1-9 on the rectangular mesh and 10 and 11 on the polar mesh. In the work here the stresses were computed on the right half in a zone-by-zone fashion. The stresses were computed in zone 1 using the stress-free conditions along the lower and right edges as boundary conditions. In addition, the shear stress was assumed to be zero along the model centerline. After the zone 1 computations the stresses were computed in zone 2. The stresses computed along line A-A in the zone 1 computations were used as boundary conditions for the lower edge of zone 2. In addition zone 2 utilized the traction-free conditions on the right edge and shear-free condition on the centerline. Computations proceeded like this from one rectangular zone to the next. The procedure was altered slightly for the finer mesh zones but the basic idea was the same. Computations then proceeded to the polar zones. Since the coordinate axes at each point in the polar mesh did not align with the x-y system, the transformed stress-optic laws, eqs. A2, were applied at each point, the constants c_1 - c_5 being different at different circumferential locations. At each point in the polar meshes the two stress-optic equations and the two equilibrium equations, in polar finite-difference form, were applied. Computations started in zone 10. The boundary conditions for the outer arc, line c-a, were determined by interpolation of results from zone 3, 5 and 6 computations. On radial line coincident with the centerline the shear stresses were set to zero. The compuations were then done in zone

11. Zone 10 computations along radial line ab and linear interpolation from zones 6, 8 and 9 computations along outer arc a-d were used as boundary conditions. Details of the computational procedure are available in ref. [A11].

Voloshin [A12] used a similar scheme in computing stresses in a tensile specimen but incorporated the compatibility equations as well. Chandrashekhara and Jacob [A13] relied on just the compatiblity equations to effect separation of stresses. The numerical approach, as opposed to a third experimental measure, to stress separation was chosen here so that a simple standard polariscope set-up could be used. Extra optical apparatus for an interferometric measure can be complicated and it is not clear oblique incidence is as accurate for fiber-reinforced materials as it is for homogeneous materials. The stress-optic coefficients and the residual birefringence data for the four plates tested are given in Table A1. As can be seen from eqs. A1 and A2, elastic property data for the material were not necessary for stress calculations.

Table A1

Optical Calibration Data for Plates(1)

	isotropic	quasi-isotropic	unidirectional	angle-ply
f_x, kPa/fringe/m	51.0	96.8	129	674
f_y, kPa/fringe/m	51.0	96.8	68	674
f_{xy}, kPa/fringe/m	51.0	96.8	57	115
N_R, fringe	0	0	0.12	0
θ_R	0	0	0	0

(1) determined from four-point bend specimens

References

A1) Pih, H. and Knight, C. E., "Photoelastic Analysis of Anisotropic Fiber Reinforced Composites," J. Composite Materials, vol. 3, June 1969, pp. 94-107.

A2) Sampson, R. C., "A Stress-Optic Law for Photoelastic Analysis of Orthotropic Composites," Experimental Mechanics, May 1970, pp. 210-215.

A3) Dally, J. W. and Prabhakaran, R., "Photo-orthotropic-elasticity," Experimental Mechanics, Aug. 1971, pp. 346-356.

A4) Bert, C. W., "Theory of Photoelasticity for Birefringent Filamentary Composites," Fibre Science and Technology, vol. 5, 1972, pp. 165-171.

A5) Cernosek, J., "On Photoelastic Response of Composites," Experimental Mechanics, Sept. 1975, pp. 354-357.

A6) Hahn, H. T. and Morris, D. H., "Anisotropic Photoelasticity with Application to Composites," Fibre Science and Technology, vol. 11, 1978, pp. 113-125

A7) Doyle, J. F., "Constitutive Relations in Photomechanics," Int. J. Mech. Sciences, vol. 22, 1980, pp. 1-8.

A8) Prabhakaran, R., "Fabrication of Birefringent Anisotropic Model Materials," Experimental Mechanics, Sept. 1980, p. 320-321.

A9) Daniel, I. M., Niro, T. and Koller, G. M., "Development of Orthotropic Birefringent Materials for Photoelastic Stress Analysis," NASA Contractor Report 105709 May 1981.

A10) Hyer, M. W. and Liu, D. "An Assessment of the Accuracy of Orthotropic Photoelasticity," NASA Contract Report 3773, March 1984.

A11) Liu, D., Stress Analysis of Pin-Loaded Orthotropic Plates Using Orthotropic Photoelasticity, Ph.D. Thesis, Virginia Polytechnic Institute and State University, Blacksburg, Virginia 24061

A12) Voloshin, A., "Stress Field Evaluation in Photoelastic Anisotropic Materials: Experimental-Numerical Technique," J. Composite Materials, vol. 14, Oct. 1980, pp. 342-350.

A13) Chandrashekhara, K. and Jacob, K. A., "Experimental-Numerical Hybrid Technique for Stress Analysis of Orthotropic Composites," Developments in Composite Materials-1, G. S. Holister, ed., Applied Science, Ch. 5, pp. 67-83.

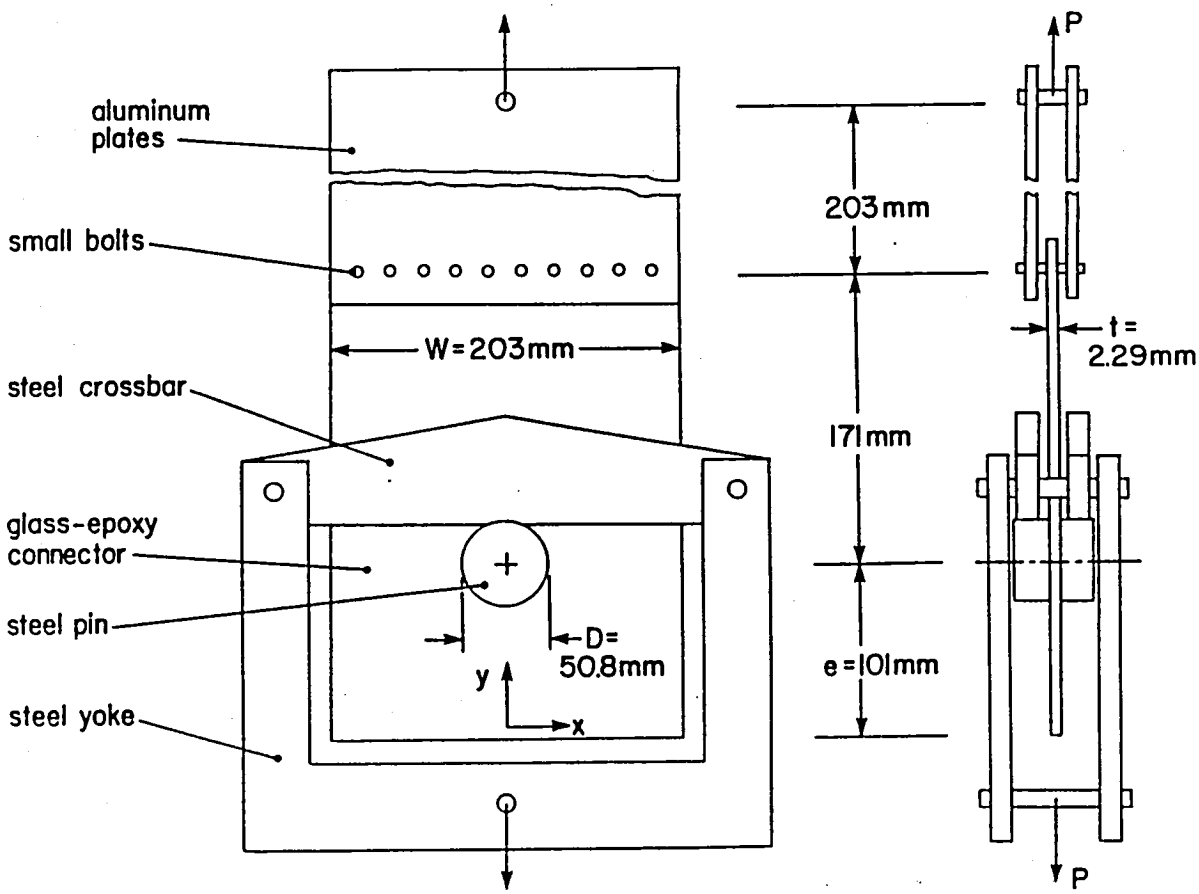

Fig. 1 Schematic of arrangement used to load plates

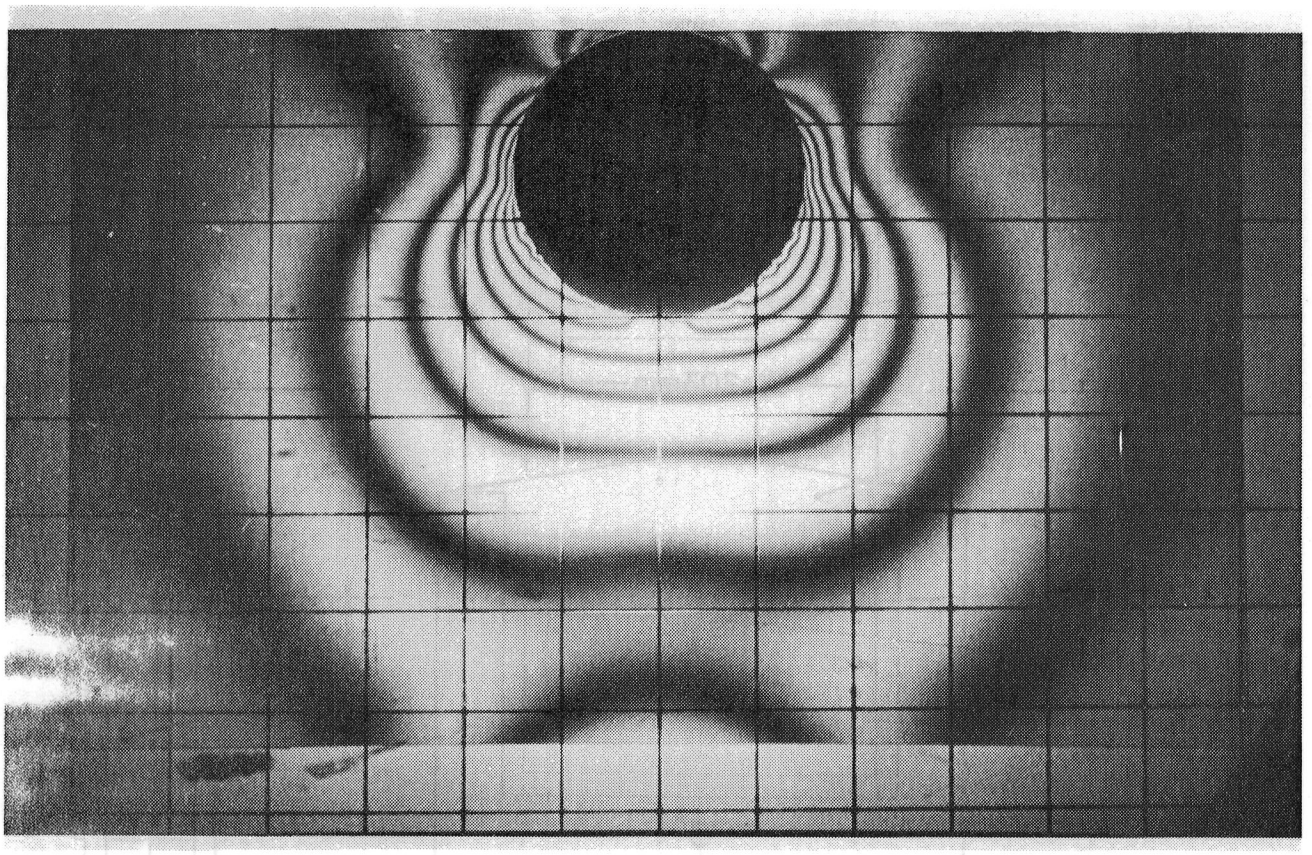

Fig. 2 Lightfield isochromatic fringe pattern, isotropic specimen, load = 1.56 kN

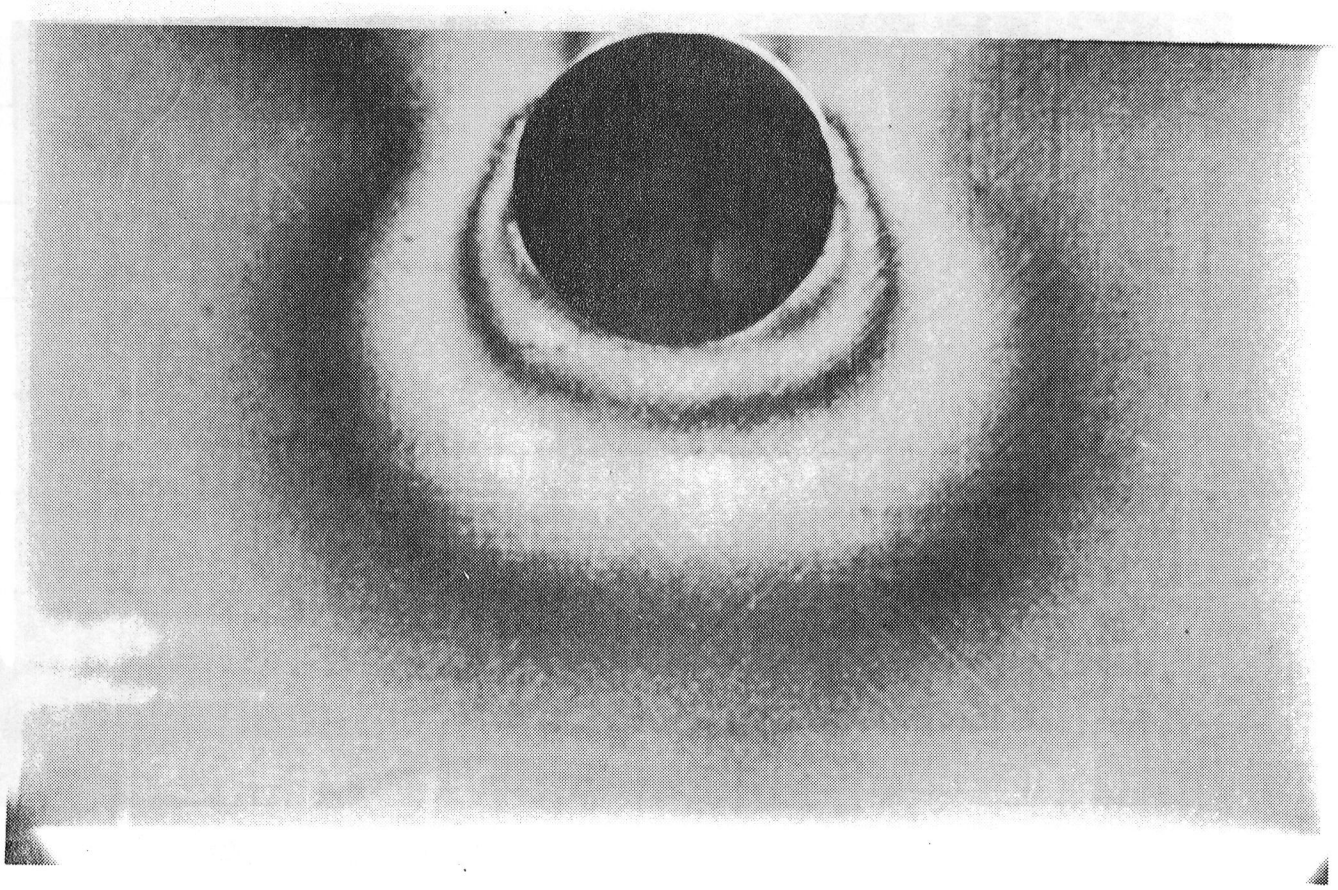

Fig. 3 Lightfield isochromatic fringe pattern, quasi-isotropic specimen, load = 5.92 kN

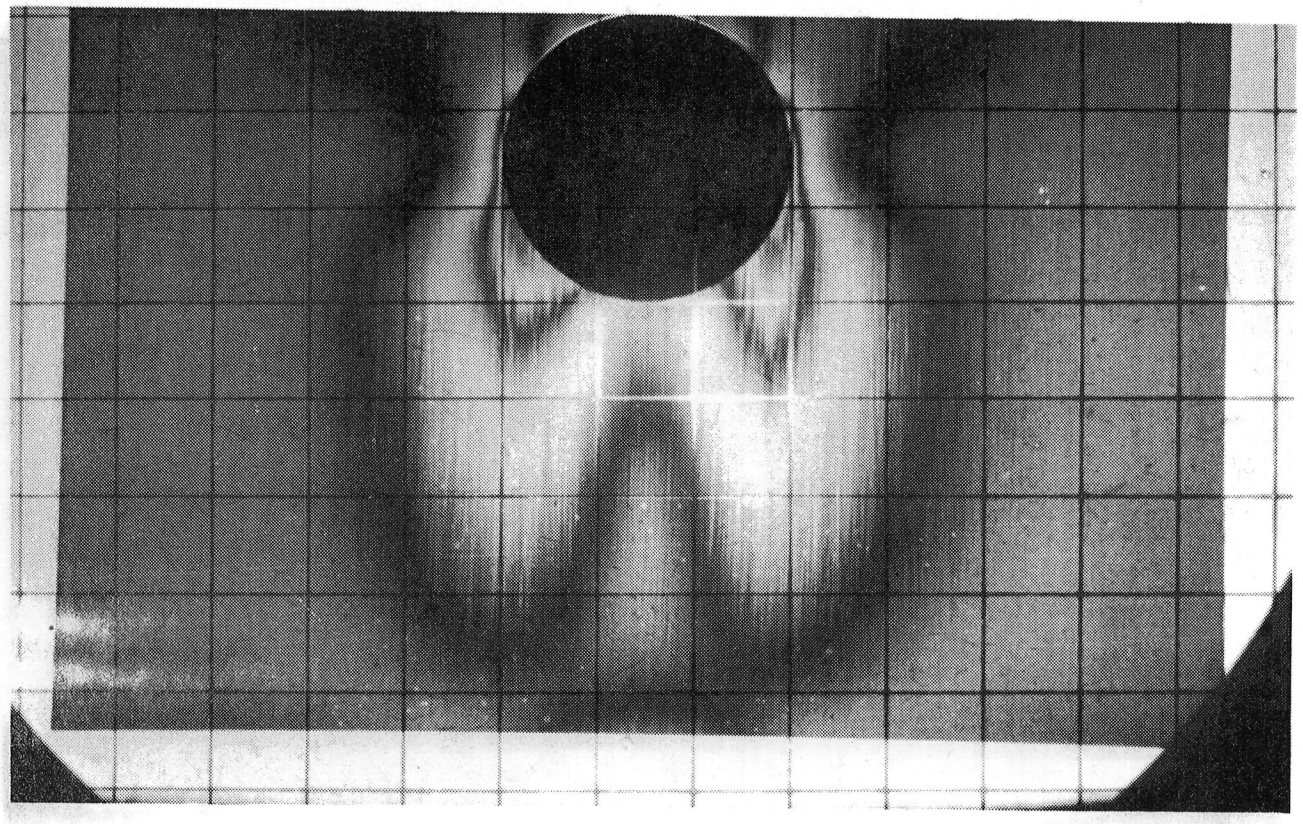

Fig. 4 Lightfield isochromatic fringe pattern, unidirectional specimen, load = 5.92 kN

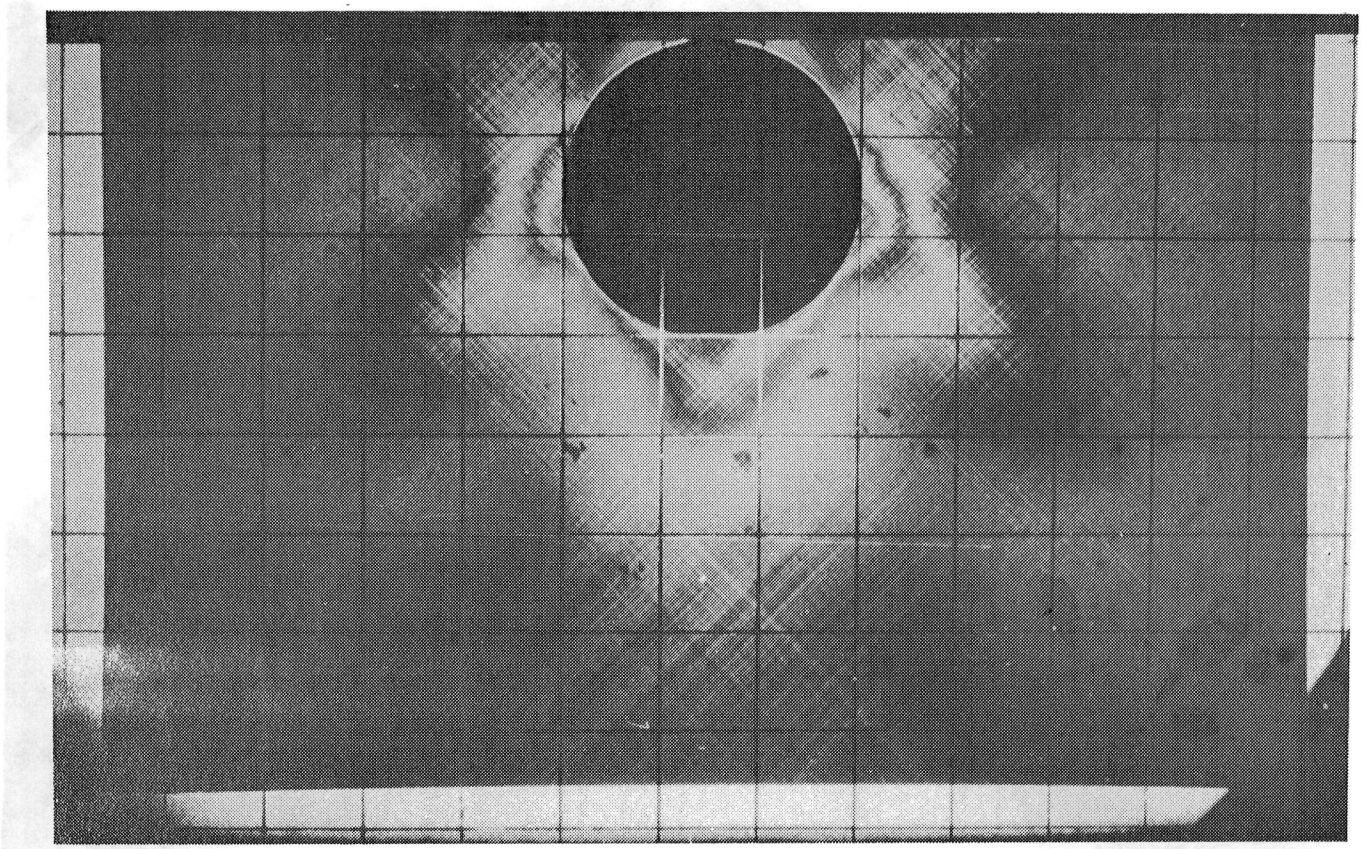

Fig. 5 Lightfield isochromatic fringe pattern, angle-ply specimen, load = 5.92 kN

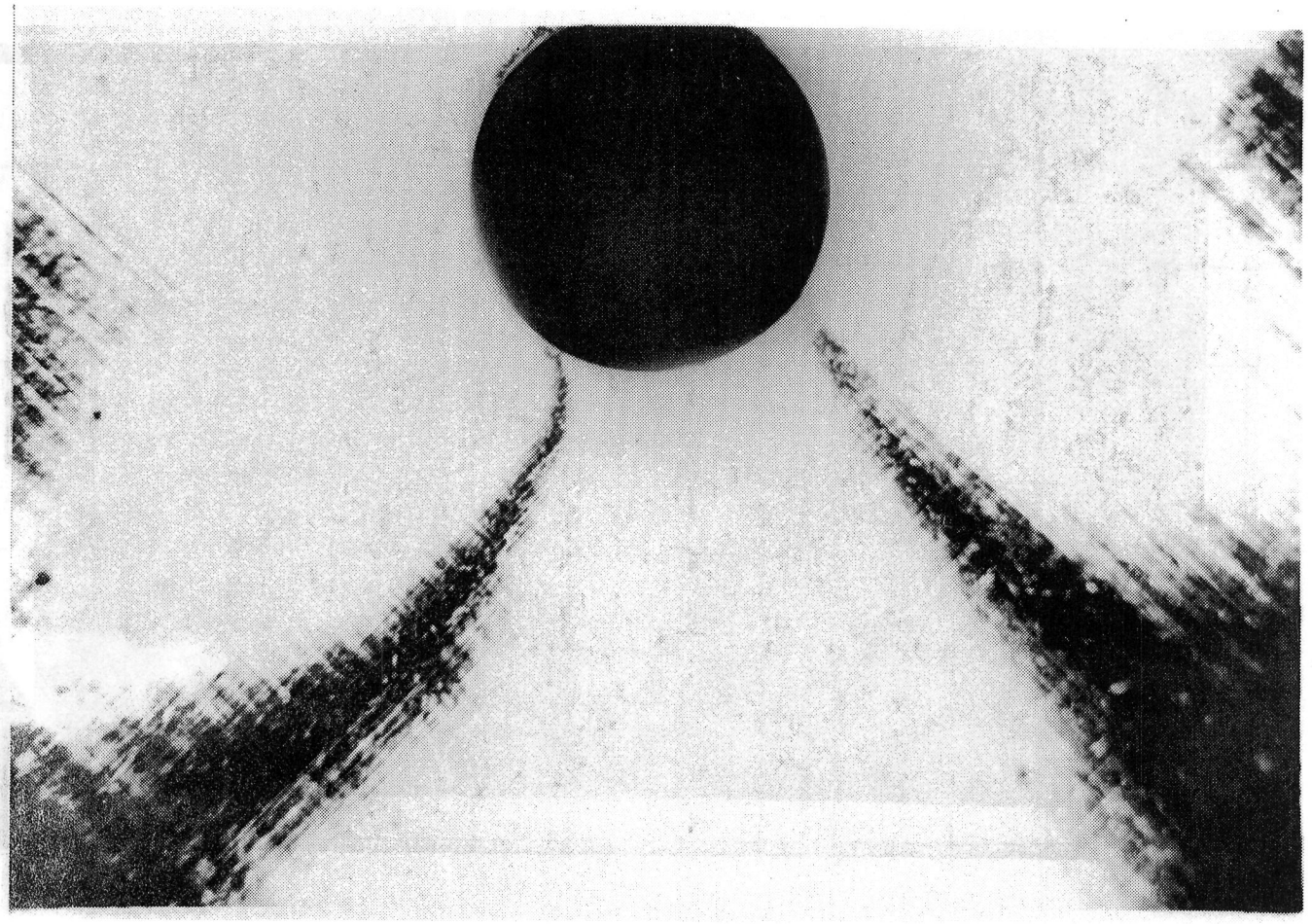

Fig. 6 Thirty degree isocline for quasi-isotropic specimen.

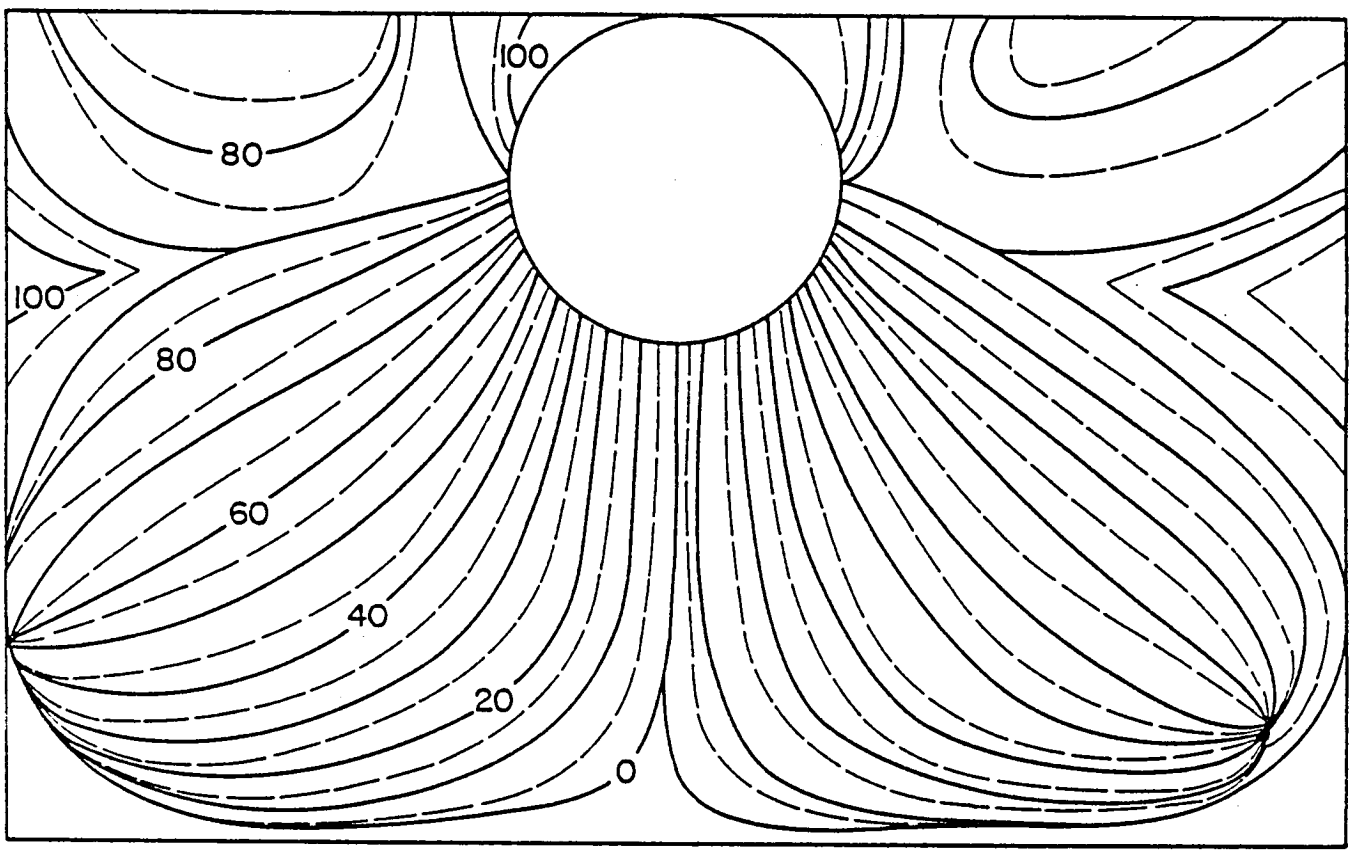

Fig. 7 Isoclinics in isotropic plate, isocline angles indicated.

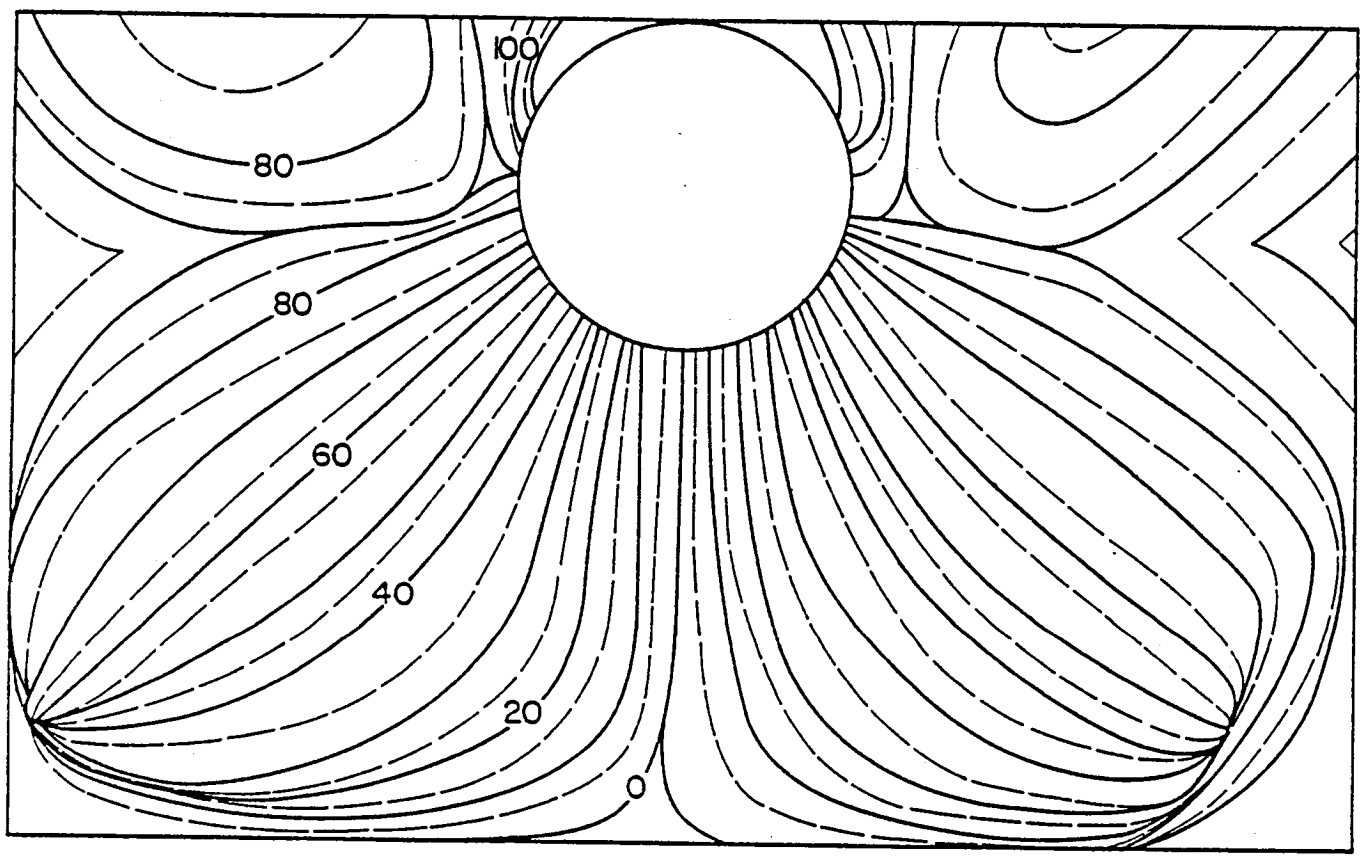

Fig. 8 Isoclinics in quasi-isotropic plate, isocline angles indicated.

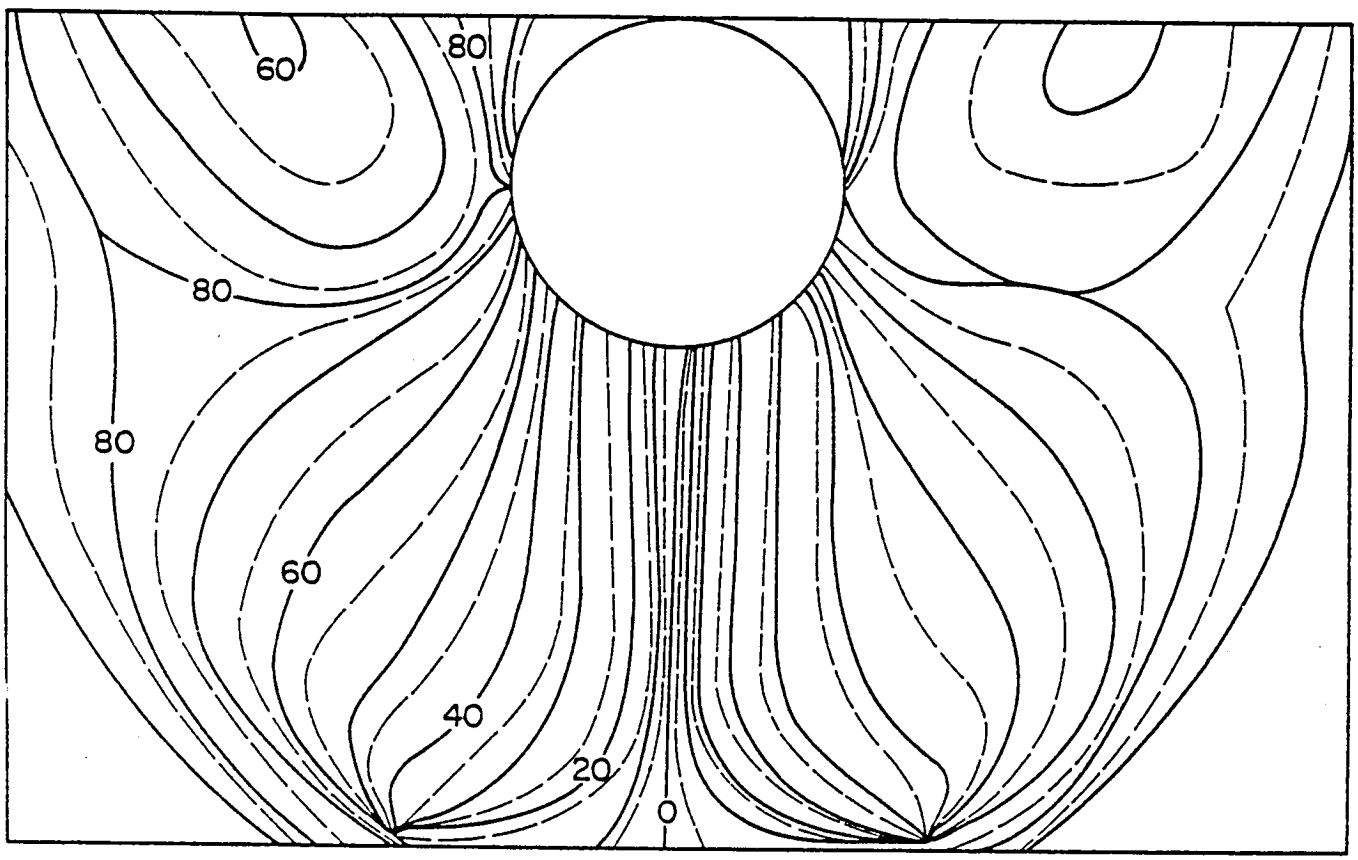

Fig. 9 Isoclinics in unidirectional plate, isocline angles indicated.

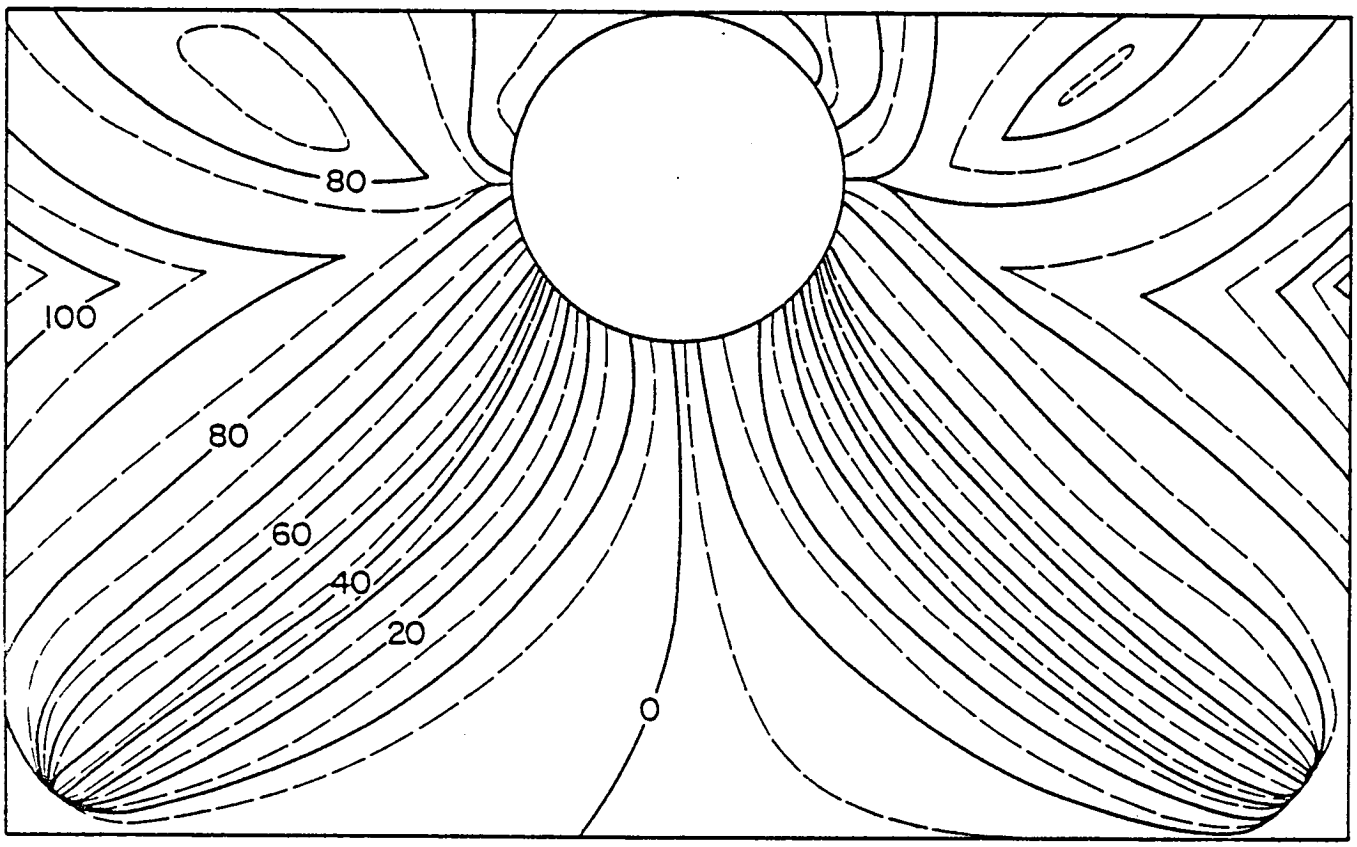

Fig. 10 Isoclinic in angle-ply plate, isocline angles indicated.

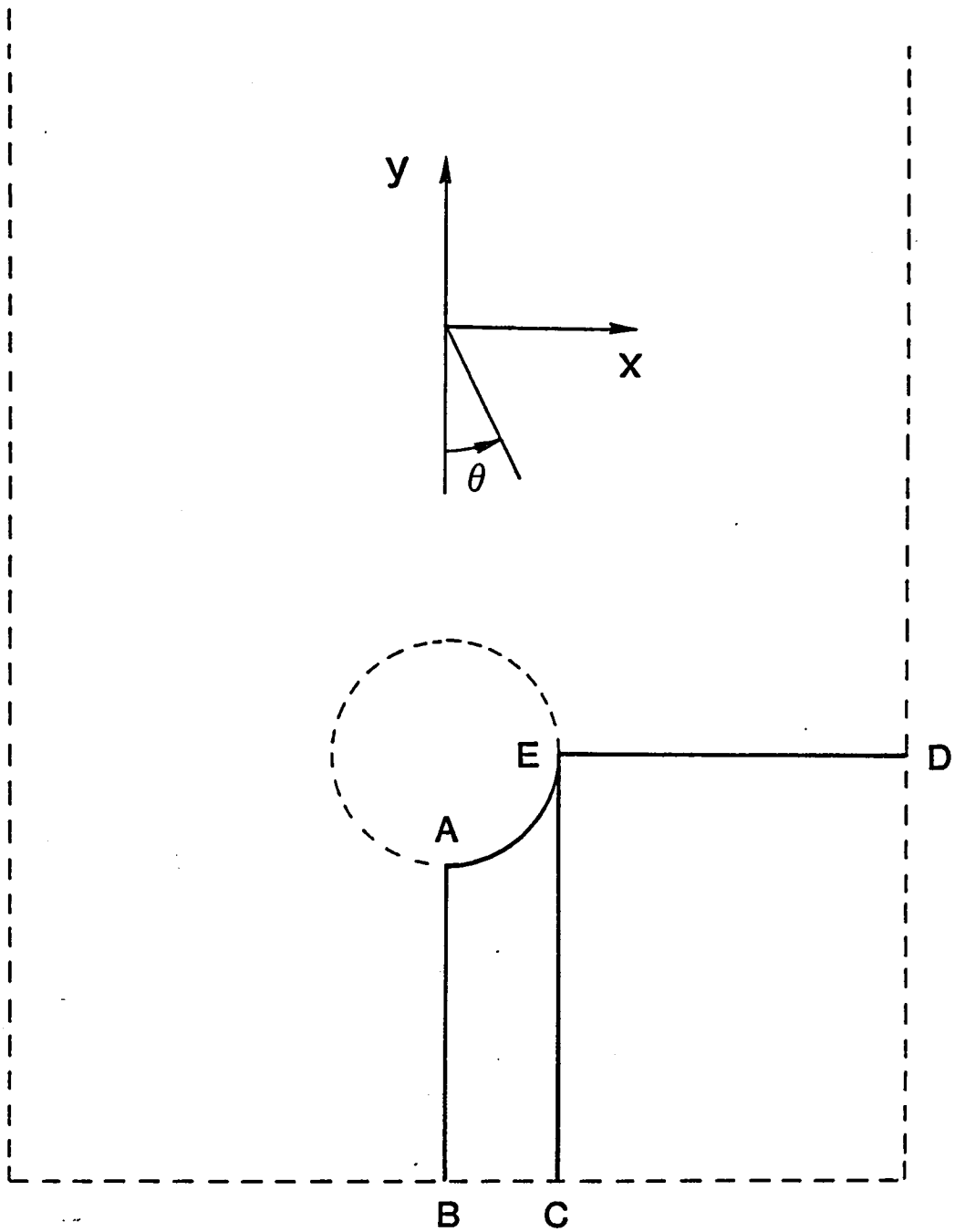

Fig. 11 Loci along which stresses are shown.

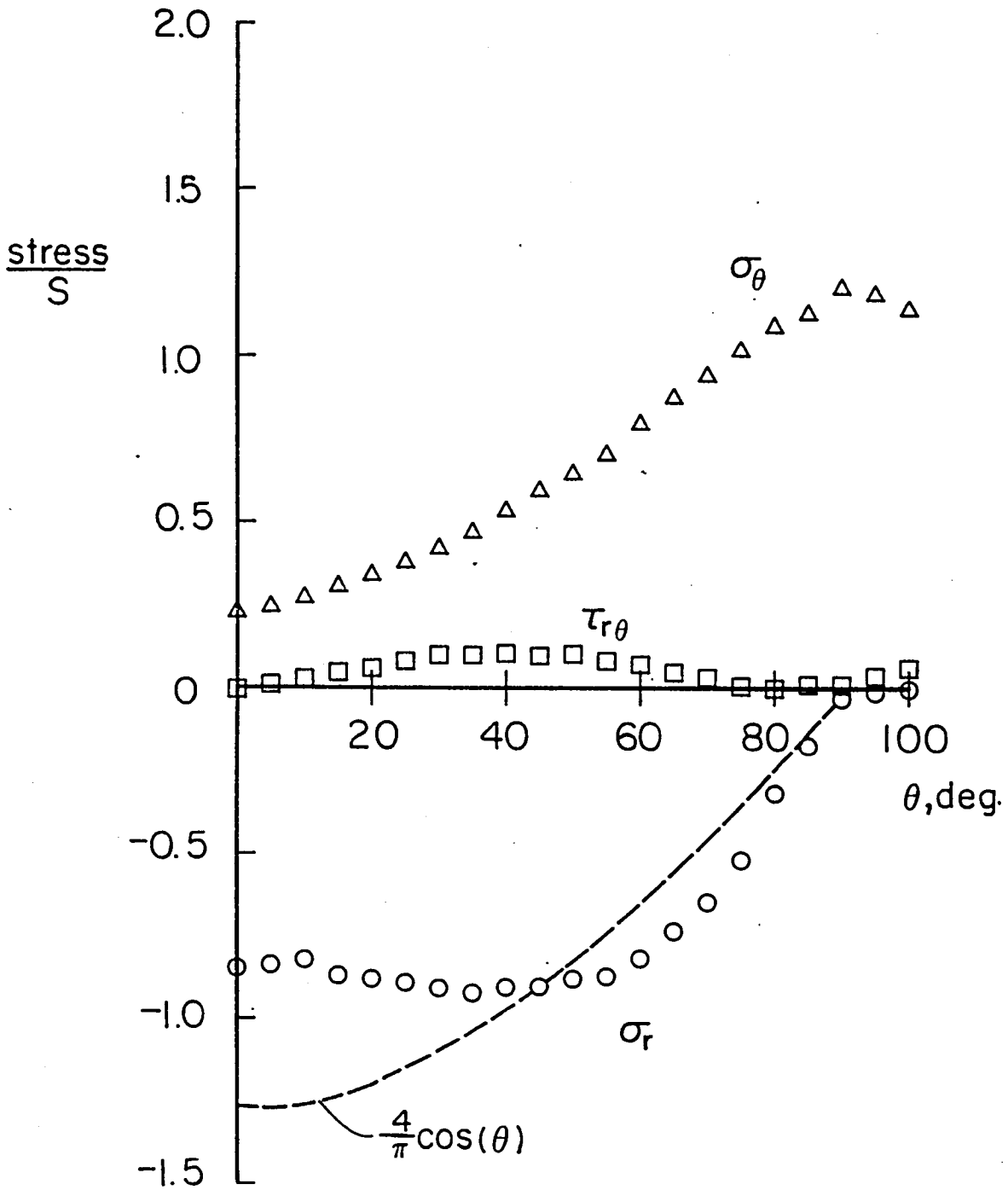

Fig. 12 Hole-edge stresses, isotropic plate.

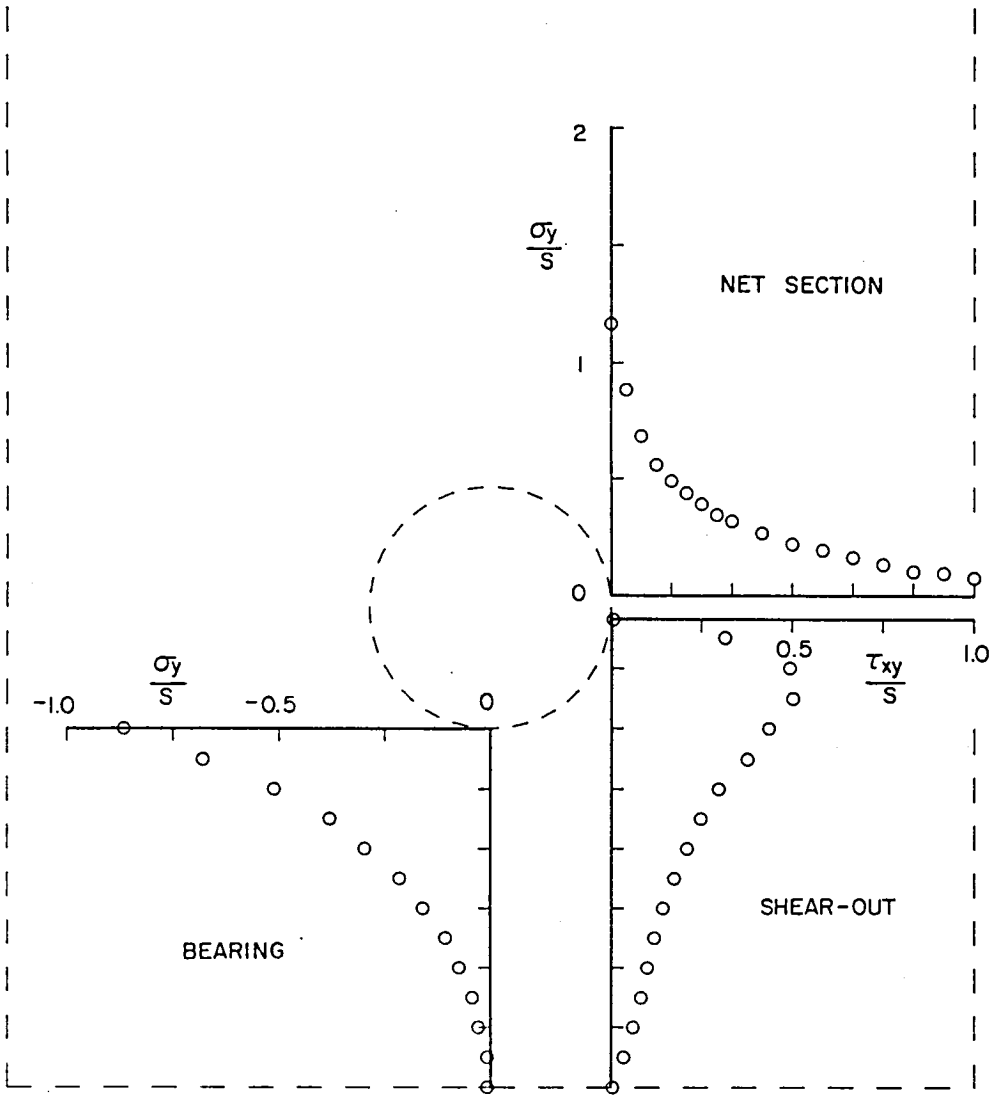

Fig. 13 Stress along various loci, isotropic plate.

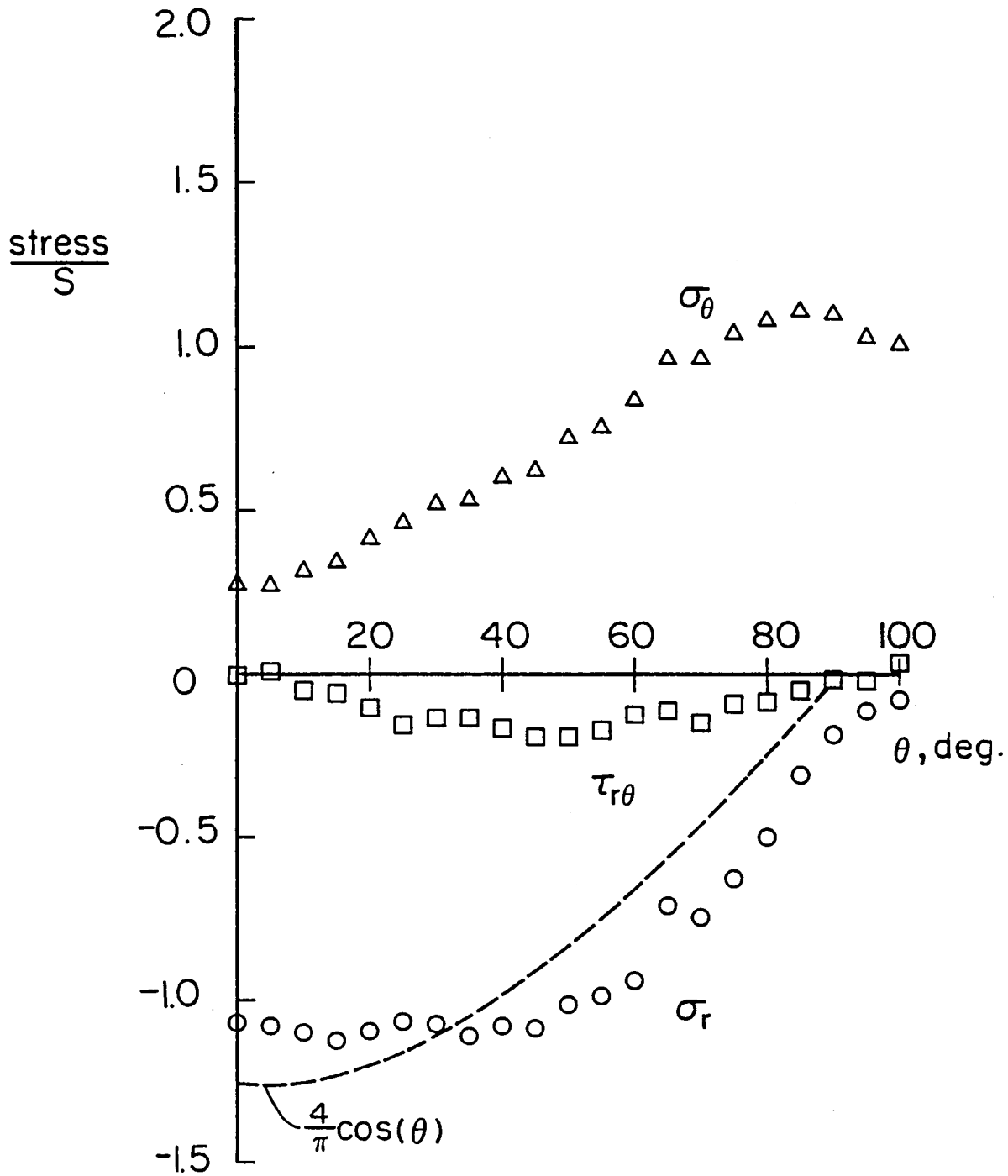

Fig. 14 Hole-edge stresses, quasi isotropic plate.

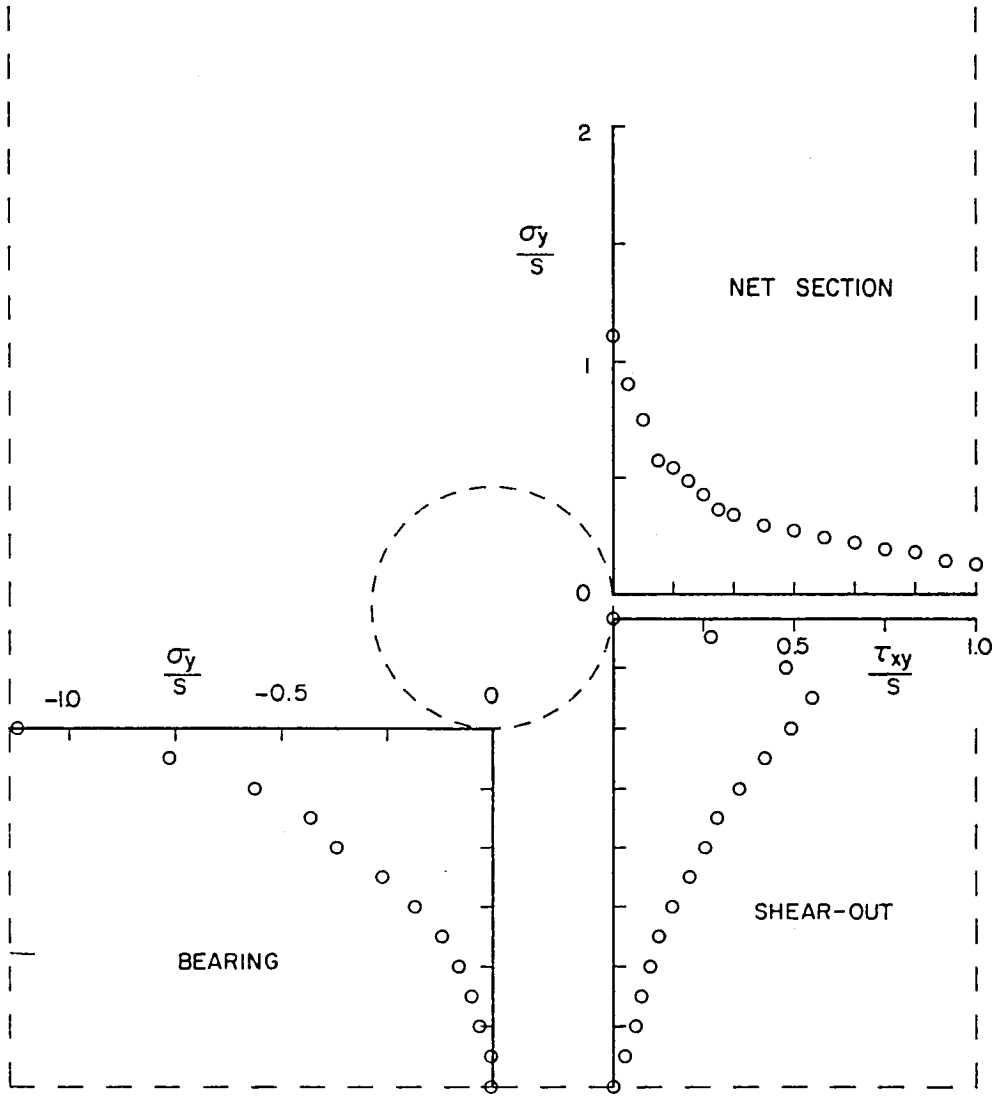

Fig. 15 Stresses along various loci, quasi-isotropic plate.

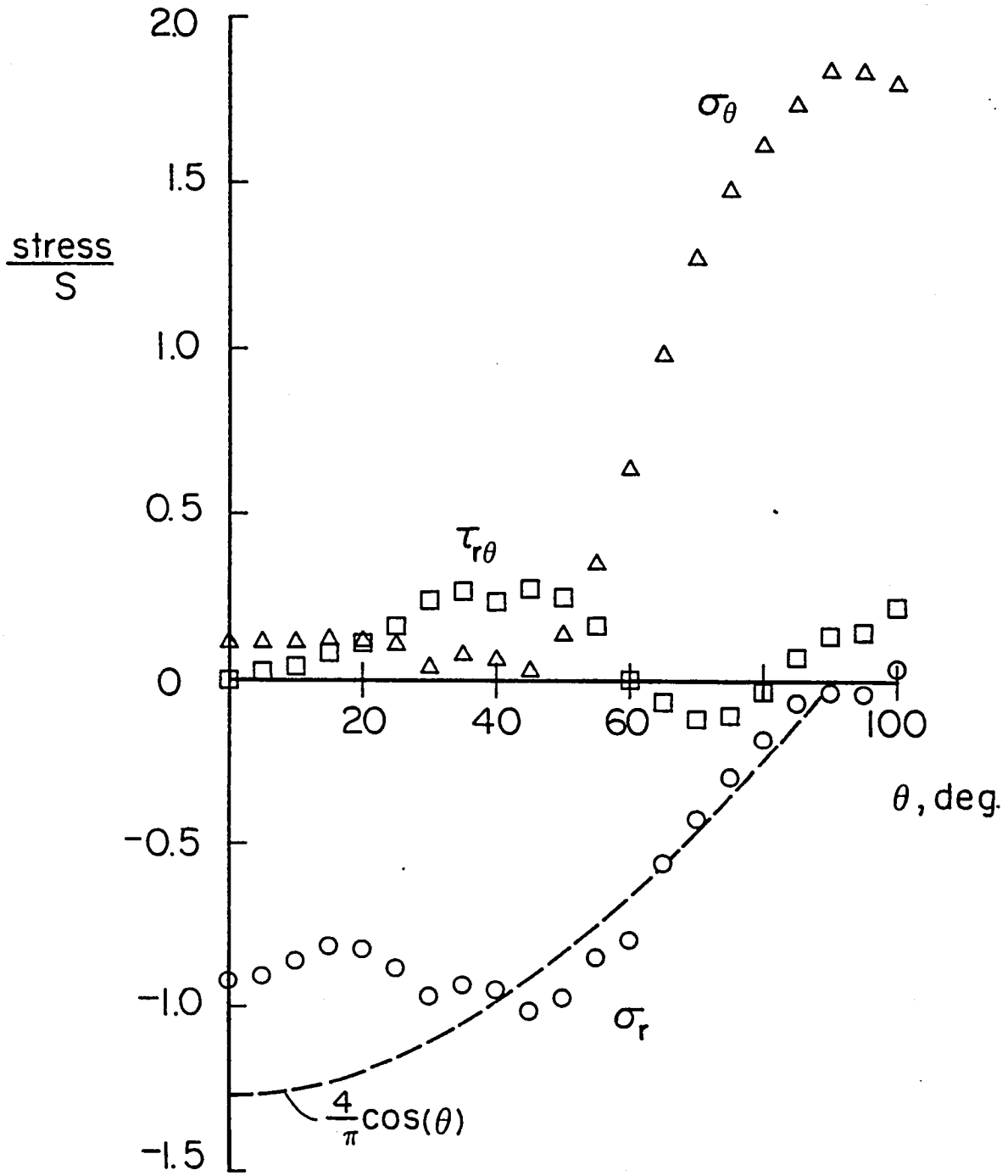

Fig. 16 Hole edge stresses, unidirectional plate.

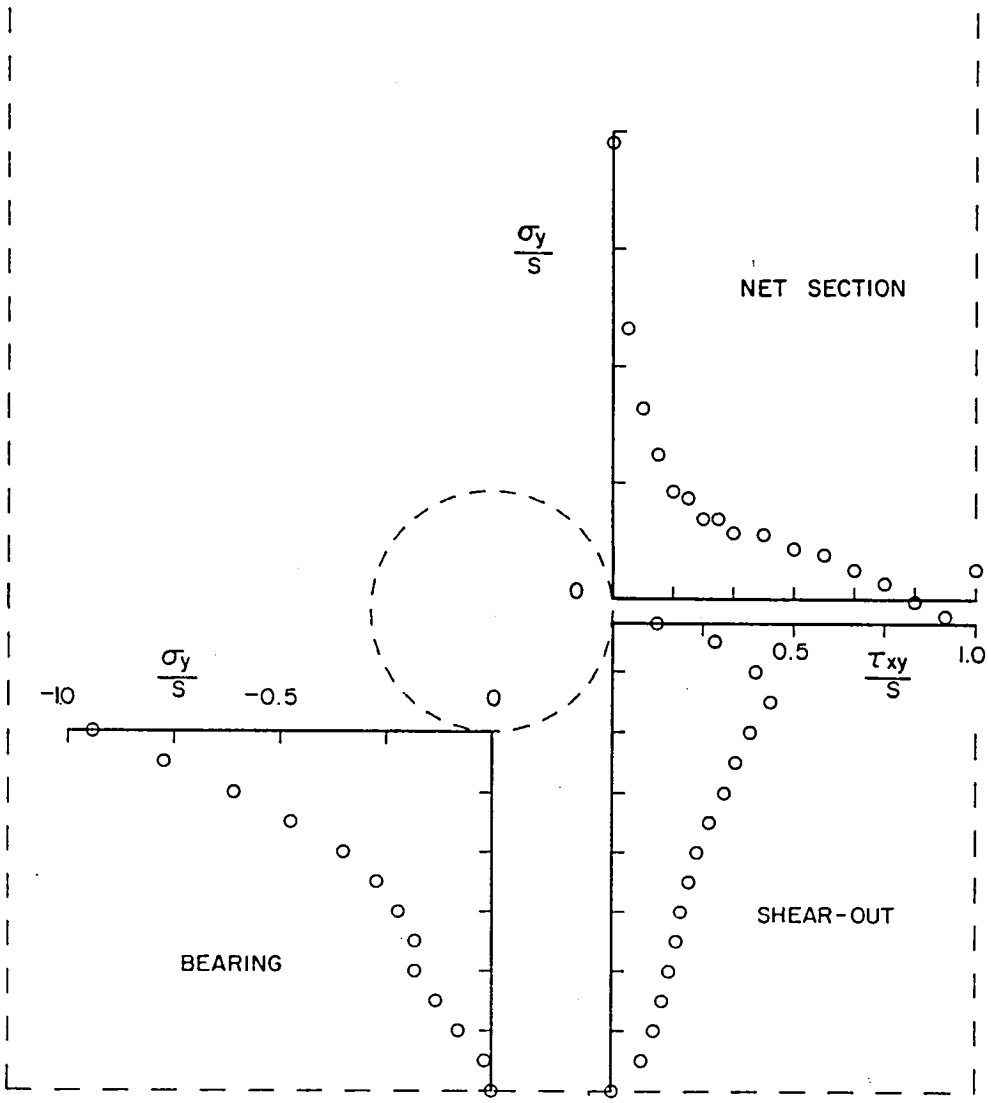

Fig. 17 Stresses along various loci, unidirectional plate.

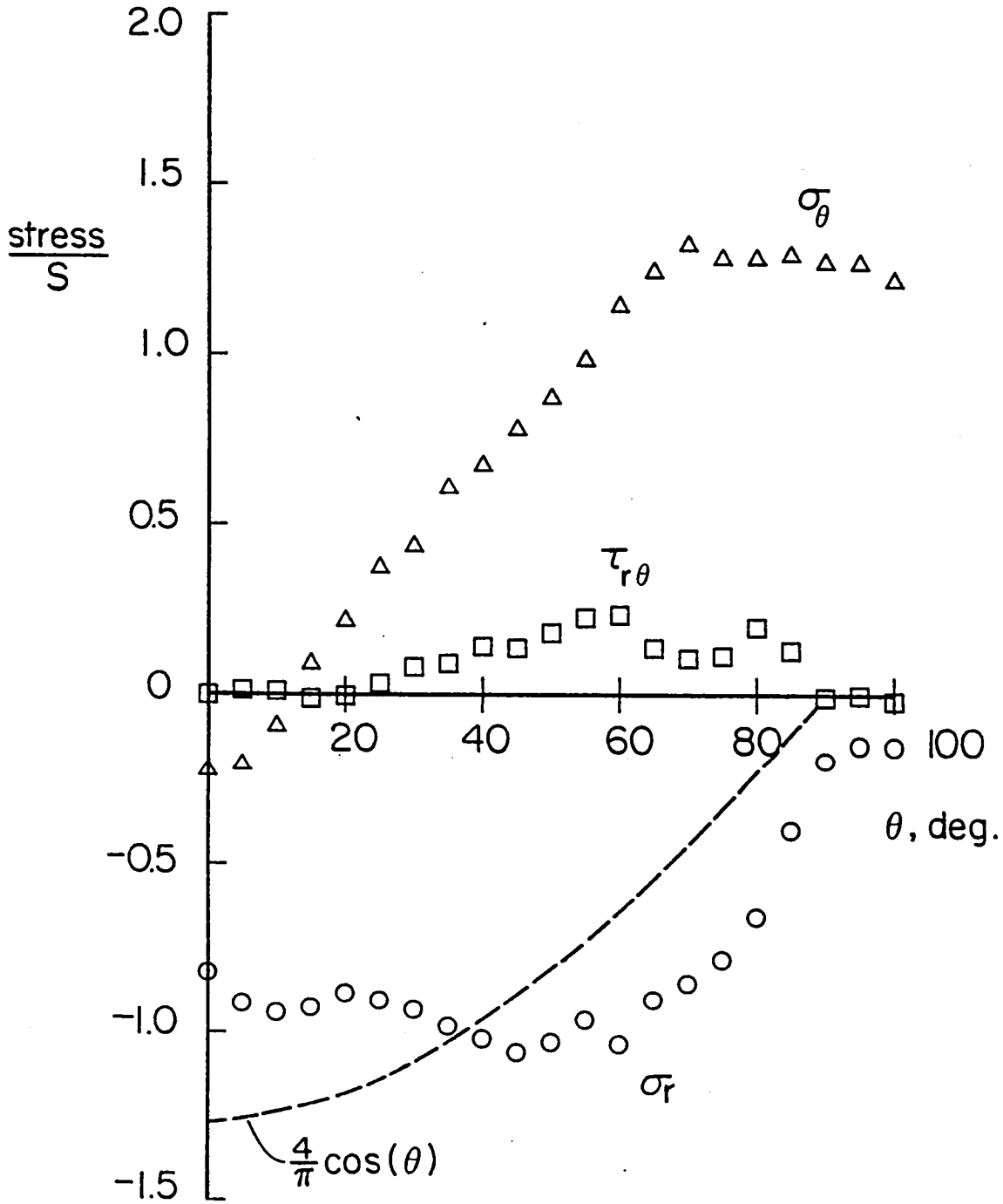

Fig. 18 Hole edge stresses, angle-ply plate.

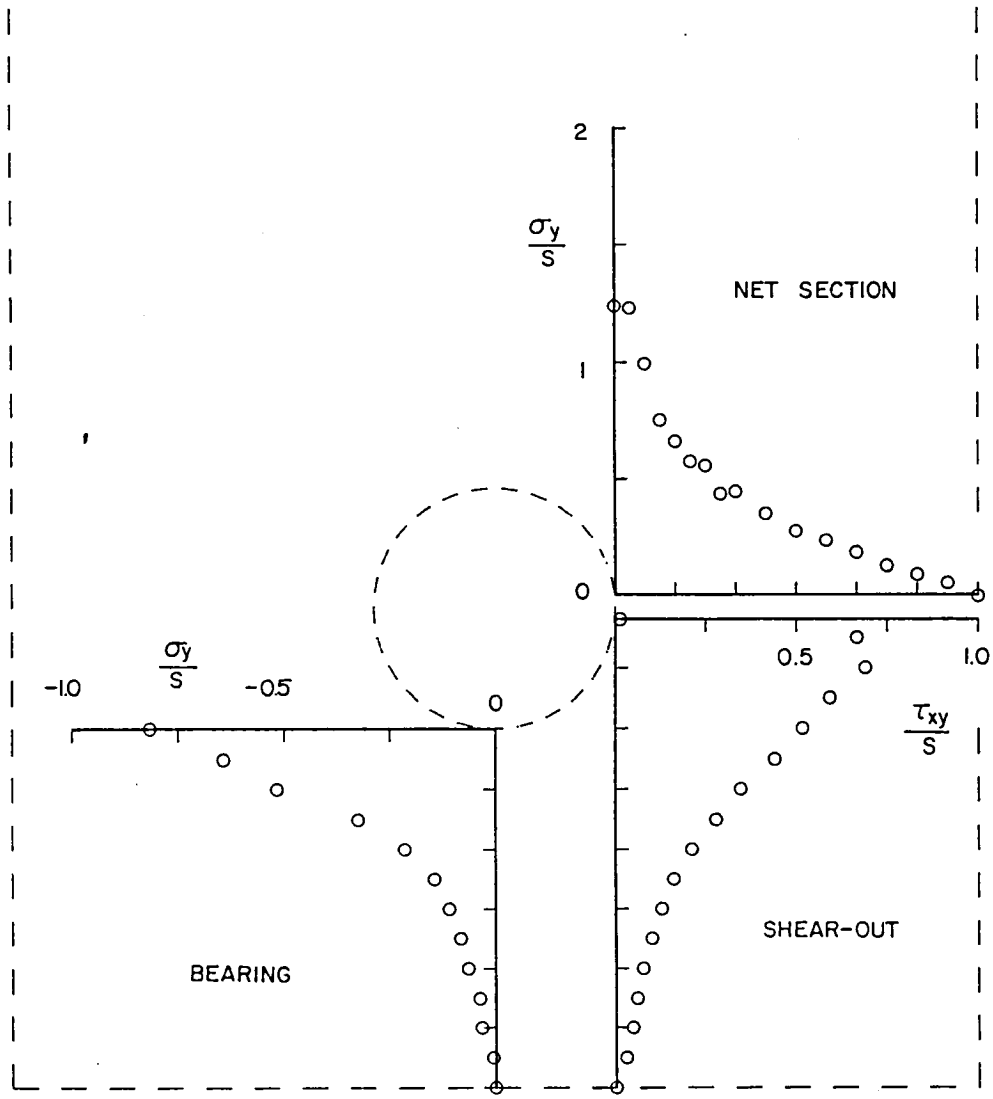

Fig. 19 Stresses along various loci, angle-ply plate.

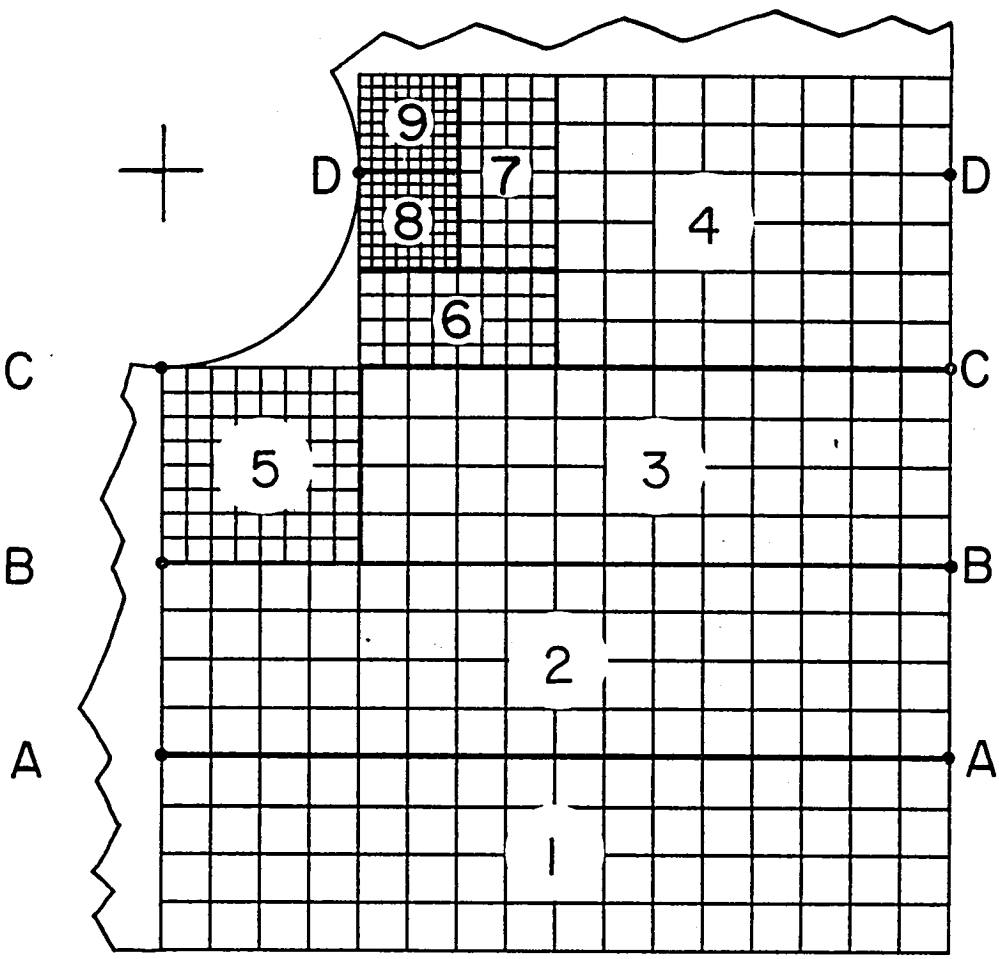

Fig. A1 Rectangular mesh

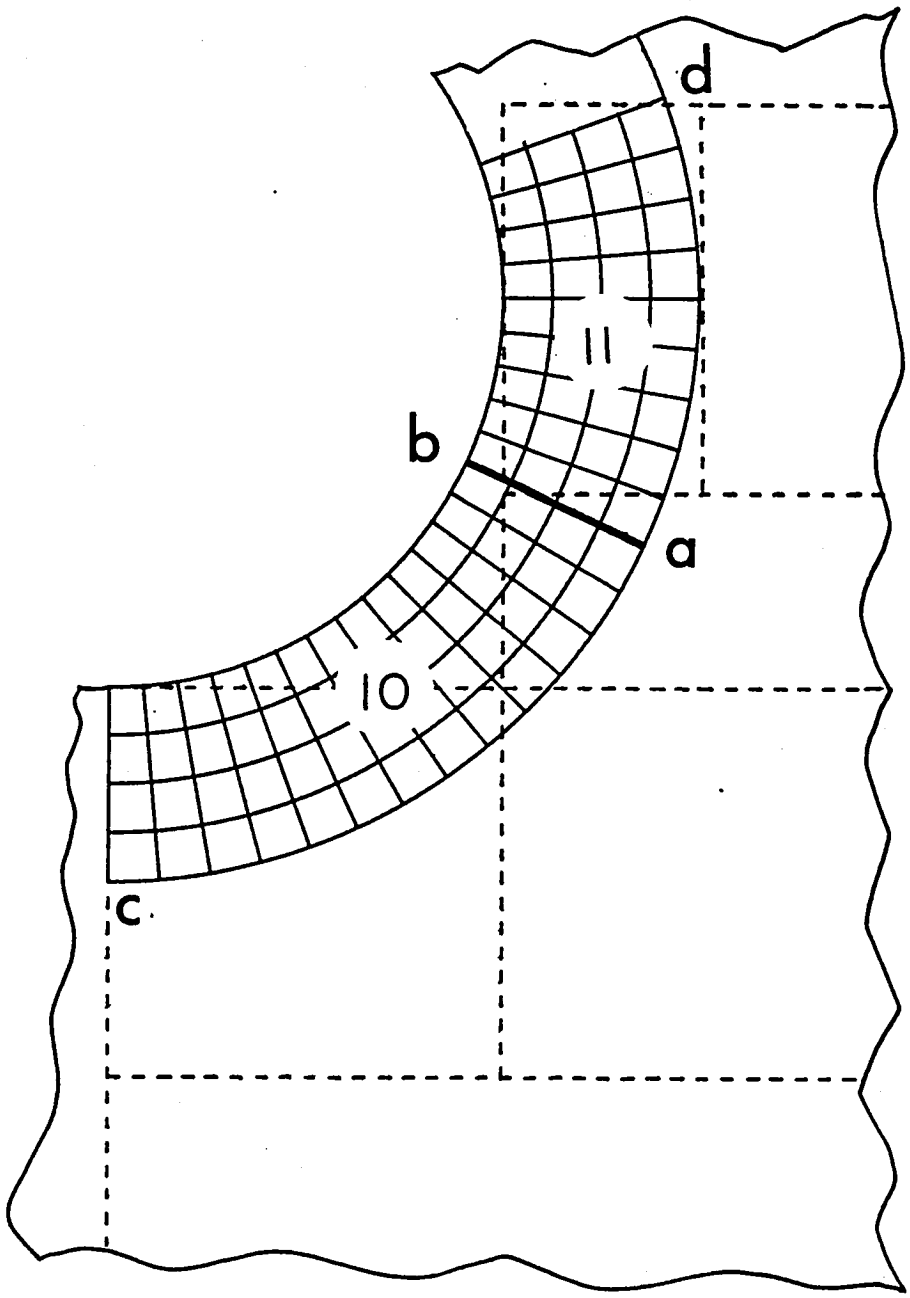

Fig. A2 Polar mesh

1. Report No.	2. Government Accession No.	3. Recipient's Catalog No.
NASA CR-172498		

4. Title and Subtitle	5. Report Date
Stresses In Pin-Loaded Orthotropic Plates Using Photoelasticity	October 1984
	6. Performing Organization Code

7. Author(s)	8. Performing Organization Report No.
M. W. Hyer D. Liu	

9. Performing Organization Name and Address	10. Work Unit No.
Engineering Science and Mechanics Department Virginia Polytechnic Institute and State University Blacksburg, VA 24061-4899	
	11. Contract or Grant No. NSG-1621

12. Sponsoring Agency Name and Address	13. Type of Report and Period Covered
National Aeronautics and Space Administration Washington, DC 20546	contractor report 8/81 - 10/84
	14. Sponsoring Agency Code 505-42-23-03

15. Supplementary Notes

The research effort which led to the results presented here was financially supported by the Structures Laboratory, USARTL (AVSCOM). The technical monitor was Donald J. Baker, NASA Langley Research Center.

16. Abstract

The stresses in transparent glass-epoxy plates loaded by a steel pin through a hole were determined experimentally using photoelasticity. The paper presents the stresses around the hole edge, across the net section, along the shear-out line, and on the centerline below the hole for quasi-isotropic, unidirectional, and angle-ply plates. Stresses in an isotropic comparison specimen are also presented. Stress concentration factors for several locations around the plates are tabulated. The paper discusses the experimental apparatus and the experimental technique. The isochromatic and isoclinic fringe patterns for the four plates are shown. An appendix presents the necessary photoelastic theory.

17. Key Words (Suggested by Author(s))	18. Distribution Statement
bolted composite joints, pin-loaded holes, composite materials, orthotropic photo-elasticity, stress concentration factors, experimental-numerical techniques, glass-epoxy	Unclassified - unlimited subject category 39

19. Security Classif. (of this report)	20. Security Classif. (of this page)	21. No. of Pages	22. Price
unclassified	unclassified	48	A03